

Dark Matter Freeze-out in a Matter Dominated Universe

BY

SALEH HAMDAN

B.S., North Carolina State University, 2009

M.S., University of Illinois at Chicago, Chicago, 2015

THESIS

Submitted as partial fulfillment of the requirements
for the degree of Doctor of Philosophy in Physics
in the Graduate College of the
University of Illinois at Chicago, 2018

Chicago, Illinois

Defense Committee:

Wai-Yee Keung, Chair

James Unwin, Advisor

Arthur Licht, Advisor

Richard Cavanaugh

Christopher Kolda, University of Notre Dame

arXiv:2108.07752v1 [hep-ph] 17 Aug 2021

Dedication

I dedicate this work to my dear mother, brother, and remaining family, without whose support this work would have been impossible.

Acknowledgements

First and foremost I wish to sincerely thank my advisor James A. Unwin for his guidance and help. I especially want to thank him for suggesting matter-dominated freeze-out as a novel scenario worth researching, which is what grew into this thesis. His guidance was vital throughout my research, writing, publishing, as well as all the other processes that academics must undertake.

I would also wish to express gratitude to my advisor Arthur (Lew) Licht, who guided me through advanced physics that was essential in completing this thesis, and was helpful and patient with me as I explored research topics. I wish to further express my gratitude toward other members of my thesis and preliminary exam committee: Richard Cavanaugh, Wai-Yee Keung, Mikhail Stephanov, and Christopher Kolda.

I am deeply thankful for the teachers I have had throughout my graduate tenure. In particular, Arthur (Lew) Licht taught me Statistical Mechanics, General Relativity, and String Theory; Tom Imbo taught me Quantum Field Theory; Richard Cavanaugh taught me Particle Physics; Wai-Yee Keung taught me Quantum Mechanics; and Mikhail Stephanov taught me Electromagnetism. No words can express the amount of gratitude and respect I hold towards them for passing on their wisdom and knowledge to me.

I would also like to thank the UIC Physics Department and the UIC Mathematics, Statistics, and Computer Science Department for accommodating me as I took classes in their departments and did research. Last, but certainly not least, I thank Fermilab for accommodating me during my early research in particle physics there.

Statement of Originality

The ideas contained in chapters of this thesis have appeared in S. Hamdan, and J. Unwin [1], arXiv:1710.03758. Additionally, Chapters 5 and 6 are expected to appear in a separate forthcoming publication. In all of the original work presented in this thesis I am responsible for the major derivations and calculations, while J. Unwin provided direction, guidance, and checks.

Summary

Dark Matter Freeze-out in a Matter Dominated Universe

A thesis submitted for the degree of *Doctor of Philosophy*.

Saleh Hamdan

University of Illinois at Chicago

The universe has evolved through several phases as its various constituents dominated its energy content. Candidate dark matter particles may have undergone freeze-out during any such phase. While the standard freeze-out scenarios have been explored during the radiation-dominated era, and more recently during scalar field decay, this work extends the study of dark matter freeze-out to a potential early period during which the universe is matter-dominated and its evolution adiabatic. Decoupling during an adiabatic matter dominated era changes the freeze-out dynamics, since the Hubble rate is parametrically different for matter and radiation domination. Furthermore, for successful Big Bang Nucleosynthesis the state dominating the early universe energy density must decay, this dilutes (or repopulates) the dark matter. As a result, the masses and couplings required to match the observed dark matter relic density can differ significantly from radiation dominated freeze-out.

Contents

Nomenclature	xiii
List of Figures	xv
1 Introduction	1
1.1 The Case for Dark Matter	3
1.2 Empirical Searches for Dark Matter	9
2 Matter Domination in the Early Universe	15
2.1 Relating Time, Scale Factor, and Temperature	15
2.2 Interpolating Friedmann Equation	19
2.3 Early Universe Scenarios with a Matter-like Species	21
3 Freeze-out of Dark Matter During Matter Domination	23
3.1 Freeze-out Temperature	24
3.2 The Boltzmann Equation	27
3.3 Freeze-out Abundance	29
3.4 Dark Matter Relic Density	31
3.5 The Dilution Factor	35
4 Constraints on Matter Dominated Freeze-out	39
4.1 Freeze-out of dark matter during matter domination	40
4.2 Freeze-out of dark matter before decay of Φ matter	42
4.3 Constraints on the reheating temperature	43
4.4 Ordering of scales	45
4.5 Summary	47
5 Beyond Instantaneous Decay	49

5.1	Decay Equations	49
5.2	Breakdown of Entropy Conservation in the Bath	51
5.3	Hubble Parameter During Decays	55
5.4	Temperature Maxima During Decay	58
6	Matter Dominated Freeze-out via the Higgs Portal	59
6.1	Dark Matter Annihilation to Standard Model States	60
6.2	Relic Density for the Scalar Higgs Portal	66
6.3	Theoretical Constraints	70
6.4	Experimental Constraints	75
7	Conclusion	79
	Bibliography	81

Nomenclature

Abbreviations

BBN Big Bang Nucleosynthesis

BE Boltzmann Equation

DM Dark matter

FLWR Friedmann–Lemaitre–Robertson–Walker

LHC Large Hadron Collider

MB Maxwell-Boltzmann

MD Matter domination

MDFO Matter dominated freeze-out

RD Radiation domination

RDFO Radiation dominated freeze-out

SM Standard Model

Symbols

α Used to parameterize thermally-averaged cross-section

β Parameter used to define matter domination

Γ_Φ Decay width of decaying species

$\hat{\gamma}$ Ratio of relativistic degrees of freedom at T_\star to T_{RH}

\mathcal{A} Ratio of a_\star to scale factor

\mathcal{T}	Ratio of t_\star to comoving time
\mathcal{T}_{EV}	\mathcal{T} when entropy violation becomes considerable
Ωh^2	Fractional critical density with Hubble parameter uncertainty h
ρ_\star	Energy density at T_\star
ζ	Dilution factor
a_\star	Scale factor at T_\star
g_*	Energy relativistic degrees of freedom
g_{*S}	Entropic relativistic degrees of freedom
H_\star	Hubble parameter at T_\star
H_{MD}	Hubble parameter when matter domination ensues
r	Fraction of energy in radiation at T_\star
s_{RH}	Entropy after dilution
s_{R}	Entropy before dilution
T_Γ	Temperature when decay ensues
T_\star	Temperature of thermal bath when decaying species evolves as matter
t_\star	Comoving time at T_\star
T_F	Freeze-out temperature
T_{BBN}	Minimum reheating temperature to fulfill BBN constraint
T_{EV}	Temperature when entropy violation becomes considerable
t_{EV}	Comoving time when entropy violation becomes considerable
T_{MD}	Temperature when matter domination ensues
T_{RH}	Reheat temperature
w	Parameter relating pressure and energy density
x_F	Dimensionless freeze-out parameter
Y_∞	Freeze-out abundance

List of Figures

1.1	Superposition of measured rotational velocities versus radial distance plots for all 21 Sc galaxies, from [10].	4
1.2	Rotation curve fits (solid line) for NGC 6503 taken from [11].	4
1.3	CMB power spectrum for varying energy content of the universe, from [18].	6
1.4	Planck Collaboration CMB temperature power spectrum [17].	6
1.5	Bullet Cluster image taken from [25].	8
1.6	Dark matter-nucleon cross-section exclusion limits from various direct detection experiments from [30].	11
1.7	Feynman diagrams for mono-X processes taken from [36].	13
3.1	Plot of dark matter mass m_X vs dilution ζ in matter dominated freeze-out.	33
3.2	Contours of $\Omega_X h^2 = 0.1$ for matter and radiation dominated freeze-out . .	34
4.1	Parameter space of matter dominated dark matter freeze-out	48
5.1	Relevant events for matter dominated freeze-out without the instantaneous decay approximation.	53
6.1	Dark Matter to Standard Model Fermions, $\varphi\varphi \rightarrow f\bar{f}$	61
6.2	Dark Matter to Standard Model Vector Bosons, $\varphi\varphi \rightarrow V\bar{V}$	63
6.3	Dark Matter to Higgs Bosons, $\varphi\varphi \rightarrow hh$	65
6.4	The total Higgs Portal annihilation cross-section.	67
6.5	Fraction of annihilation cross-section to Standard Model particles	68
6.6	Constraints and relic density contours for $T_\star = 10^7$ GeV and $T_\star = 10^4$. . .	74
6.7	Three processes in the CMS search for invisible Higgs decays, from [37]. .	76
6.8	Experimental and theoretical bounds for $T_\star = 10^7$ GeV and $T_\star = 10^4$ GeV.	77
7.1	Figure from J. Bramante and J. Unwin JHEP 1702 (2017) 119	80

Chapter 1

Introduction

This chapter introduces the main topic of this thesis.

The current dark matter density is measured to be $\Omega_{\text{CDM}}h^2 = 0.115$ [2]. There has been many proposals for particles which might account for dark matter, ranging from axions, Weakly Interacting Massive Particles (WIMPs), Strongly Interacting Massive Particles (SIMPs), to the variety of Supersymmetric (SUSY) particles and beyond [3]. With little known about which, if any, candidate may be dark matter, it is prudent to take a model-independent approach to exploring the parameter space of this elusive constituent of our universe.

Dark matter may have once been in thermal equilibrium with the photon plasma; such dark matter candidates are termed thermal, and will be the focus of this thesis. An effective method for exploring the validity of a thermal dark matter candidate is to compute its freeze-out abundance. Because an interaction becomes much less likely whenever $\Gamma \lesssim H$, where Γ is the interaction rate of a particle and H is the Hubble parameter, dark matter annihilations become much less likely (“Frozen-out”), preserving a relic abundance we may measure today. The goal of such calculations is to investigate the parameter space of a species of particles, such as its mass and interaction strength, consistent with the thermal history of the universe and the abundance we measure of such a particle today. An example of the fruitfulness of such a method is the Lee-Weinberg bound for a stable, cold neutrino species, $m_\nu \gtrsim 2$ GeV [4].

Although freeze-out calculations have been performed for dark matter candidates, these calculations have typically been carried out assuming freeze-out occurred either during an era of the universe when relativistic particles dominated the energy content of the universe [5], referred to as the radiation domination phase, or while a scalar field undergoes coherent oscillations as it decays with high adiabicity violation (one may also view this latter scenario as the decay of a massive unstable species of particles) [6, 7]. While these scenarios are feasible, there are no violations of known cosmological or physical principles for freeze-out to have occurred during an adiabatic era of the universe when non-relativistic matter dominated its energy content, referred to as the matter domination phase. It is quite possible that dark matter indeed has frozen-out during a matter domination phase of the universe. This is because $\rho_M/\rho_R \propto a^{-3}/a^{-4} \propto a$, where ρ_M is the energy density of decoupled (from thermal bath), non-relativistic matter, ρ_R is the energy density of radiation, and a is the scale factor. Hence, the energy density of decoupled matter tends to grow relative to that of radiation.

The thesis is structured as follows: in the remainder of the introductory chapter we make the case for adopting the dark matter hypothesis and review the methods for searching for dark matter. In Chapter 2 we discuss some pertinent background material, rewrite the Friedmann equation in a manner conducive to studying matter domination and radiation domination limits, and give a non-technical overview of the matter domination freeze-out scenario. Chapter 3 is devoted to a rigorous treatment of freeze-out during matter domination. We then move on to discussing the constraints on the matter-dominated freeze-out scenario in Chapter 4. Since much of our analysis in Chapters 3 and 4 makes use of the instantaneous decay approximation, in Chapter 5 we demonstrate that this approximation is well justified, and show where it is less reliable. Following the model-independent approach in Chapters 3 and 4, we apply this analysis to a specific Higgs Portal model in Chapter 6, and argue that this portal to dark matter provides a viable scenario. We summarize and conclude this thesis in Chapter 7.

1.1 The Case for Dark Matter

Until a future discovery sheds light on the precise nature of dark matter, it is more of a concept than a physical object. It is a label physicists use to describe the gap between their suppositions about Nature and what it actually shows them. In the early 19th century Neptune was considered “dark”; it was just a hypothesis of the astronomers Urbain Le Verrier and John Couch Adams to describe anomalies in the orbit of Uranus [8]. Once the Berlin Observatory used a refractory telescope to observe it, Neptune went from a hypothesis to a planet in fact. The hypothesized planet *Vulcan*, which was also predicted by Le Verrier to explain the anomalous precession of the perihelion of Mercury, was never discovered [8]. Instead, the General Theory of Relativity explained the anomalous precession, and “Vulcan” was no more. This example provides an illuminating tale for physicists studying DM. Just as in the past, physicists today confront a major discrepancy between simple suppositions about Nature versus what we factually observe. Nevertheless the existence of a cold (non-relativistic) form of matter that very weakly interacts with baryonic matter is practically a scientific certainty, though its precise nature remains elusive. In this section I will highlight the case for the existence of such matter, commonly referred to as “dark matter” (DM).

As early as 1933, the astronomer Fritz Zwicky, using the virial theorem, observed that “the average density in the Coma system would have to be at least 400 times larger than that derived on the grounds of observations of luminous matter,” and that if that were the case, “dark matter is present in much greater amount than luminous matter” [9]. Although Zwicky’s argument applied to a cluster of galaxies, the principles apply just as well to any stable gravitational system; for example individual galaxies. Indeed one would expect from Newtonian gravity that the tangential velocity v_t around a spherical mass distribution to behave as

$$v_t(r) = \sqrt{\frac{GM(r)}{r}}, \quad (1.1)$$

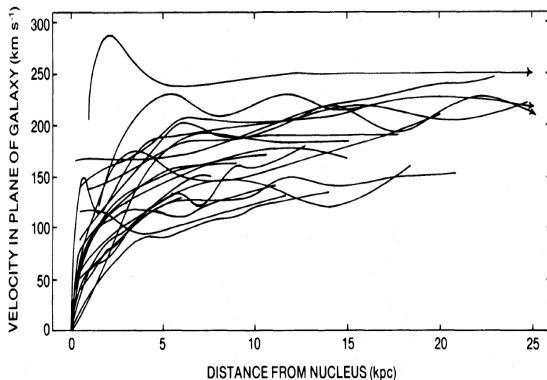


Figure 1.1: Superposition of measured rotational velocities versus radial distance plots for all 21 Sc galaxies taken from [10]. Remarkably, rotational velocity flattens out near disk radius.

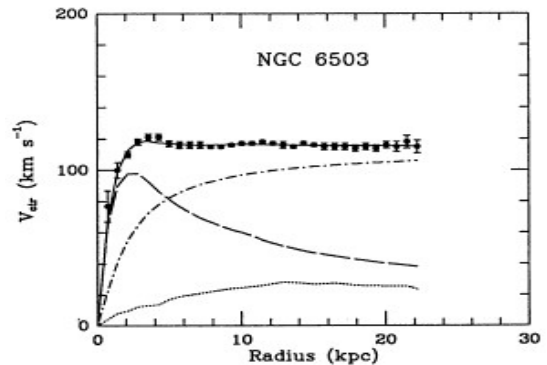


Figure 1.2: Rotation curve fits (solid line) for NGC 6503, from [11]. Rotation curves for visible matter (dashed), gas (dotted), and dark halo (dashed-dotted) also shown.

where $M(r)$ is the enclosed total mass within the radial distance r . Thus if the mass of a galaxy is concentrated in its disk, $M(r)$ should be roughly constant outside the disk, and $v_t(r \gtrsim R_{\text{disk}}) \propto r^{-1/2}$ [12]. Instead a flattening of the tangential velocity is observed as seen in Figure 1.1 taken from Rubin et al. [10]. This indicates that $M(r) \propto r$ around the disk, and hence there must be more mass in a galaxy than its luminous matter as seen in Figure 1.2 taken from Begeman et al. [11].

The essence of the problem of the galactic rotational curves is one of a high mass-to-light ratio, M/L . More mass is measured in galaxies than what we would expect from the light we observe from them [13]. But what if that mass came from baryonic objects with low luminosity? Certainly low luminosity objects exist in galaxies, such as planets, dwarf stars, and even black holes. The class of baryonic matter that may make up the missing mass in the galaxy were termed massive astrophysical compact halo objects, or MACHOs. Yet early objections to MACHOs making up the missing mass in galaxies were published [14], and by the mid-2000s the EROS-2 collaboration had shown using micro-lensing that MACHOs can only make up a maximum of 8% of the Milky Way halo

mass fraction [8, 15]. Furthermore, the baryonic budget (the relic fractional density of baryons, Ω_b) which is calculated from primordial nucleosynthesis considerations ($\Omega_b = 0.04 \pm 0.02$), inferred from the cosmic microwave background (CMB) power spectrum ($\Omega_b h^2 = 0.02273 \pm 0.00062$), as well as measured from galaxy clusters ($\Omega_b = 0.04$) indicates that it is too small to accommodate a MACHO explanation for the galactic rotational curve problem [16].

These findings suggest that a solution to the galactic rotational curve problem requires a fundamental shift away from known physics. The hypothesis of dark matter provides an elegant solution to this problem, yet that is not its most compelling evidence. What began as a hypothesis to explain the missing mass in galaxies has now become part of a standard cosmological model called Λ CDM, which assumes that the General Theory of Relativity to be correct, and includes dark energy (represented as the cosmological constant, Λ , to explain the accelerating expansion of the universe) and cold DM to describe a consistent big bang cosmology. Λ CDM makes precise predictions about the acoustic power spectrum of the CMB, which is essentially the photons reaching us from the surface of last scattering, or when photons decoupled from the rest of matter and the universe became transparent. The CMB temperature anisotropies give an acoustic power spectrum that is sensitive to the energy content of the universe as can be seen in Figure 1.3. The measured CMB power spectrum from the Planck Collaboration [17] fits the Λ CDM prediction with stunning precision as shown in Figure 1.4, thus providing compelling evidence for the existence of DM.

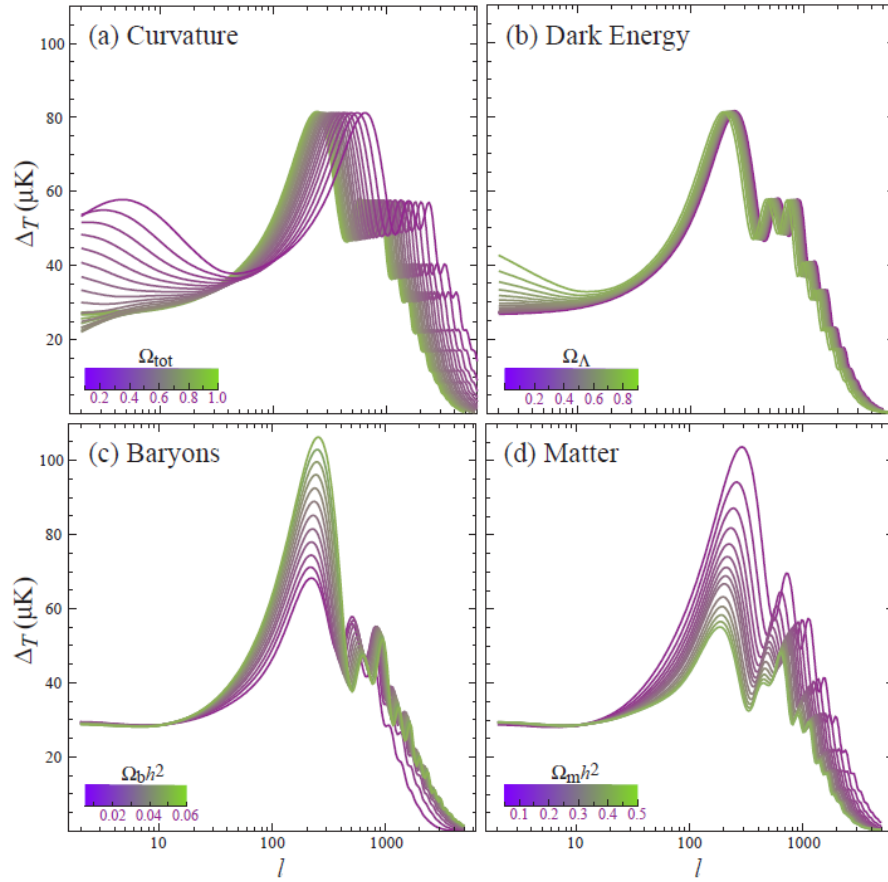


Figure 1.3: CMB power spectrum for varying energy content of the universe, from [18].

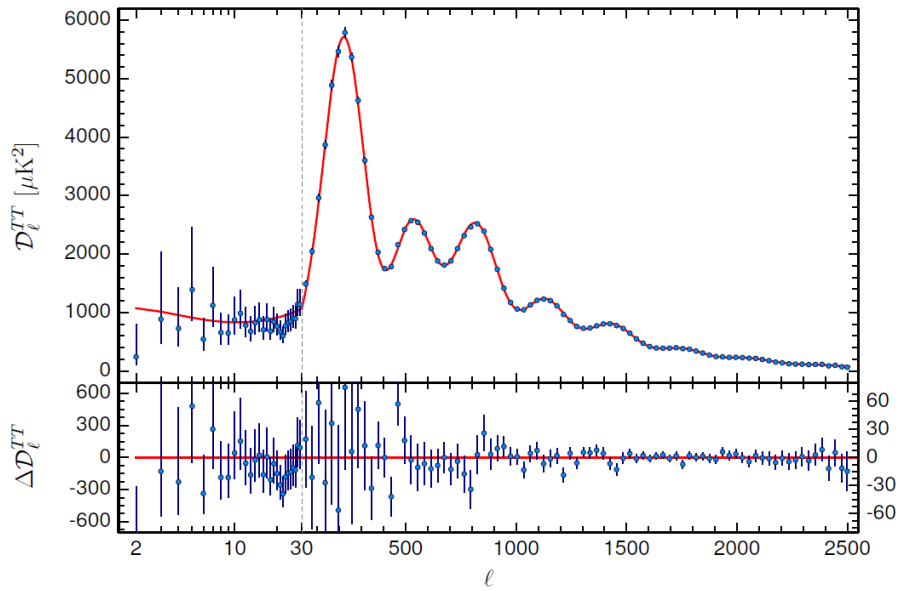


Figure 1.4: Planck Collaboration CMB temperature power spectrum [17]. Upper panel shows Λ CDM fit (solid red); lower panel shows residuals with respect to this model.

Further strengthening the case for DM is large scale structure formation in the universe. It had been known by the early 80s that the perturbations in the CMB were incompatible with the formation of galaxies and galaxy clusters in a universe composed of only baryonic matter, and that including weakly-interacting massive particles (WIMPs, a candidate DM class) in the energy profile of the universe can aid structure formation [19]. Since then computer simulations have demonstrated that Λ CDM can successfully predict the large scale structure we observe today in the universe [20–22], and have been important in modeling the structure of DM halos [23]. Simulations have also played a significant role in ruling out that hot dark matter (which is relativistic at decoupling, such as neutrinos) could be responsible for the DM density [24], thus in this thesis DM shall only refer to cold dark matter.

Finally, no case for DM would be complete without mentioning a research article boldly titled, “A direct empirical proof of the existence of dark matter.” Clowe et al. [25] analyzed the merging cluster 1E0657-558, also known as the Bullet Cluster, which is composed of two galaxy clusters merging together. Individual galaxies in a merging cluster behave as collisionless particles, whereas the intracluster plasma experiences ram pressure and emits X-rays [25]. If there was no dark matter, one would expect the gravitational potential to track the spatial configuration of the plasma, since it forms the dominant baryonic mass content of clusters. On the other hand, since dark matter only weakly interacts, it is expected to track the collisionless individual galaxies. Therefore a spatial decoupling of the X-ray emissions and gravitational potential provides compelling evidence that the bulk of mass in galaxy clusters is dark. This spatial decoupling is precisely what Clowe et al. found when they viewed the X-ray emissions from the Bullet Cluster using the Chandra telescope, and used gravitational weak lensing to probe how the gravitational potential was spatially distributed, as shown in Figure 1.5.

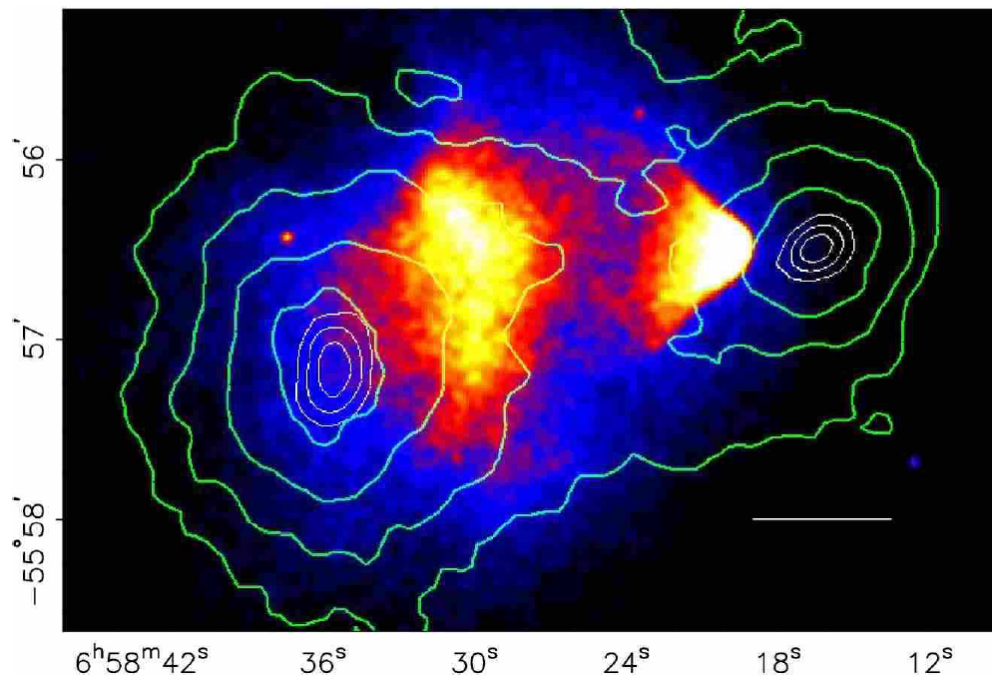


Figure 1.5: Bullet Cluster image taken from [25]. The coloring represents X-ray emissions as taken by Chandra. The green lines are reconstructed gravitational weak lensing gradients. The white bar represents 200 kpc at the distance of the cluster.

Although the precise nature of DM is currently unknown, galactic rotational curves, the baryon budget, the CMB power spectrum, large scale structure formation, and the Bullet Cluster provide compelling evidence that the existence of DM is a near scientific certainty. The evidence for dark matter, not all of which we presented here, has even led some physicists to identify its hypothesis along the lines of a Kuhnian scientific revolution [26, 27]. While other theories have emerged to explain the apparent missing mass in galaxies, most notably Modified Newtonian Dynamics (MOND) [28], these theories do not provide the same explanatory power that the Λ CDM model does for the disparate phenomenon we observe. Le Verrie’s tale demonstrates that a healthy dose of skepticism is prudent in science, but we believe that a vigorous hunt for DM through theoretical and empirical means is well warranted and exceedingly likely to inaugurate a new particle into physics, beyond the Standard Model (SM).

1.2 Empirical Searches for Dark Matter

The compelling evidence for the existence of DM has prompted several empirical efforts to detect it. We have already described the analysis of the Bullet Cluster which boasts a direct empirical proof of DM, yet the search is still on for a direct signal of DM that illuminates its precise nature [29]. The major experimental efforts can be classified into three categories: direct detection, indirect detection, and collider searches [30]. In this section we will describe these three methods and present the current bounds they give on DM parameters.

Direct detection experiments rely on observing recoils from potential DM scatterings off nuclei, in particular elements such as Xenon, Germanium and Argon, which have high atomic numbers which enhances the DM-nucleon cross-sections ($\sigma_N \propto A^2$) for certain interactions. Several factors go into predicting the rate of events that direct detection experiments should expect. Specifically, the differential event rate (with typical units of $\text{kg}^{-1}\text{day}^{-1}\text{keV}^{-1}$ or ‘dru’ standing for differential rate units) is given by [16, 29]

$$\frac{dR}{dE_R} = \frac{\rho_0}{m_N m_{\text{DM}}} \int_{v_{\text{min}}}^{v_{\text{esc}}} v f(v) \frac{d\sigma_N}{dE_R}(v, E_R) dv. \quad (1.2)$$

where ρ_0 is the local DM energy density, m_N and m_{DM} are the nucleon and DM masses respectively, $\frac{d\sigma_N}{dE_R}$ is the differential cross-section for elastic DM-nucleon scattering, $f(v)$ is the DM speed distribution in the detector frame, v_{esc} is the local escape speed in the galactic rest frame, and v_{min} is the minimum velocity that can cause recoil energy E_R . Equation (1.2) is integrated from E_T , the threshold energy that the detector is capable of measuring to infinity, and it presents the various particle physics and astrophysical inputs involved in direct detection.

As far as the particle physics input, the DM-nucleon differential cross-section encodes information about the potential interactions that DM may have with quarks. This is done by using an effective Lagrangian approach that may include generic spin-dependent and spin-independent terms [16]. In moving from quark-DM interactions to nucleon-DM cross-sections, uncertainties are introduced via the nuclear form factors and hadronic matrix elements [16]. So long as dark matter's nature does not stray far from known effective field theoretic principles, this effective Lagrangian approach warrants confidence.

Astrophysical parameters are also involved in modeling direct detection experiment outcomes. In eq. (1.2) the local DM energy density is calculated by using a model of the Milky Way DM halo (which incorporate fitting of rotation curves), and it is predicted to have the standard value of $\rho_0 \simeq 0.3 \text{ GeVcm}^{-3}$, though modeling uncertainties can cause this value to vary by a factor of 2 [16]. $f(v)$ is also traditionally taken to be Maxwellian and isotropic, and although modeling efforts have been made to relax these assumptions, it nevertheless introduces modest uncertainties in bridging theory and experiment [16]. Finally, the upper limit of integration in eq. (1.2) is $v_{\text{esc}} = \sqrt{2\Theta(R_0)}$, where $\Theta(R_0)$ is the local gravitational potential, and particles of speed greater than v_{esc} are expected not to be gravitationally bound to the Milky Way [16].

The lower bound of integration, v_{min} depends on the sensitivity of the detector. The typical bounds that direct detection experiments produce have a sharp fall on the lower mass end ($m_{\text{DM}} \ll m_N$) of the DM-nucleon cross-section exclusion limits as seen in Figure 1.6 taken from [30]. Below a threshold recoil energy that a particle of speed v_{min} produces [16], the experiment is not sensitive enough to measure this recoil which explains the sharp fall near lower mass in Figure 1.6. On the other hand, Figure 1.6 shows that towards higher masses ($m_{\text{DM}} \gg m_N$) the exclusionary limits of direct detection experiments also become weaker because the total rate is proportional to the number density of DM, implying that for fixed ρ_0 , the number density scales as $1/m_{\text{DM}}$ [16].

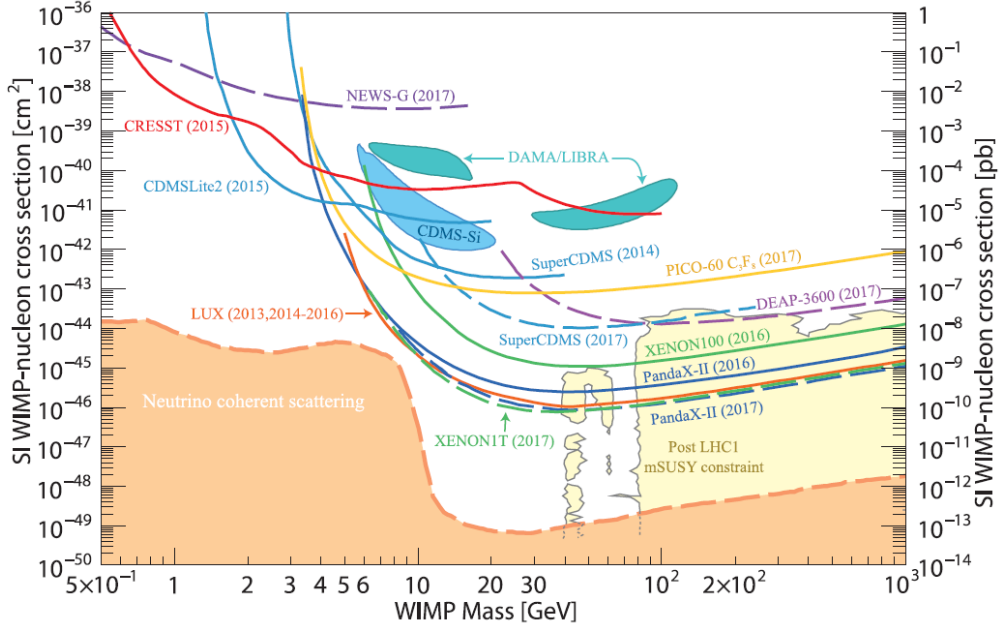


Figure 1.6: Dark matter DM-nucleon cross-section exclusion limits from various direct detection experiments taken from [30]. Black contours provide context for common SUSY models integrating constraints of ATLAS Run 1.

Despite the difficulty of separating background events from true DM scatterings, direct detection experiments currently provide among the strongest bounds on DM candidates. Nevertheless, distinguishing DM-nucleon interactions will become much more challenging when the “neutrino floor” is reached as indicated by the orange shaded region in Figure 1.6. Beyond the neutrino floor background events caused by neutrino scatterings become difficult to discriminate from DM scatterings.

Indirect detection experiments search for byproducts of possible DM annihilations from regions expected to have higher concentrations of DM such as the Sun, dwarf spheroidal galaxies of the Milky Way, or the Milky Way center [8, 16, 29]. The byproduct searches include neutrinos, antimatter, and gamma rays [16]. Focusing on gamma rays, the differential flux expected from DM annihilations is given by [29]

$$\frac{d\Phi}{d\Omega dE} = \frac{(\sigma v)_{\text{ann}}}{8\pi m_{\text{DM}}^2} \frac{dN}{dE} \int_{\text{l.o.s}} ds \rho_{\text{DM}}^2(\vec{r}(s, \Omega)), \quad (1.3)$$

where $(\sigma v)_{\text{ann}}$ is the DM annihilation cross-section, $\frac{dN}{dE}$ is the energy spectrum of photons from DM annihilations, and the integral is of the DM energy density squared taken over the line of sight.

Note that eq. (1.3) depends on the DM energy density profile in the galaxy, which is a source of astrophysical uncertainty. Particle physics uncertainties come from the annihilation cross-section and the expected number of photons produced through various annihilation channels. Definitive signals for DM annihilations would be a pair of gamma rays with the same energy equal to candidate mass m_{DM} [16]. Conversely, in the absence of excess signals, exclusionary limits are obtained by observing fluxes from a given source and using eq. (1.3) to obtain constraints on the DM annihilation cross-section [29].

The final experimental method for probing DM we will discuss are collider searches. In particle accelerators such as the Large Hadron Collider (LHC), high energy beams of particles are collided and the byproducts of such collisions are analyzed. Collider triggers only directly detect charged particles and photons, thus DM, which is expected to be electrically neutral, cannot be probed directly by these experiments [31]. Nevertheless a signature of missing energy from mono-X searches or decay width measurements provide an exciting prospect that DM had been created, and further guide our efforts at directly studying DM.

The strategy of mono-X searches are to look for high transverse momentum p_T events alongside missing transverse energy (e.g. [29, 31–35]). The high transverse momentum can be in the form of jets, vector bosons, or even Higgs bosons. The Feynman diagrams for these processes can be seen in Figure 1.7 taken from [36]. An example of a definitive signal from these types of searches would be a mono-photon event where a high- p_T photon is observed without any corresponding leptons [31].

Another method that collider searches use to look for missing energy is decay width analysis. By observing decays of a particle, it is possible to discern the fraction of decays going to an invisible sector by comparing the total and observed widths [29, 37].

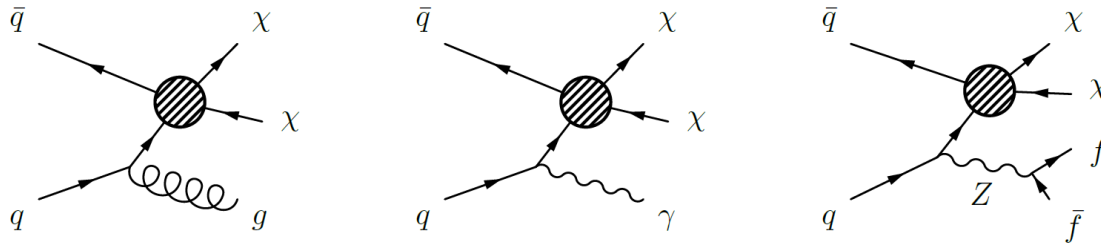


Figure 1.7: Feynmann diagrams for mono- X processes taken from [36].

The Higgs boson decays offer a particularly promising search for DM since the Higgs may directly couple to it. We will study this model called the Higgs Portal in closer detail in Chapter 6, where we highlight that collider searches are especially effective in constraining DM with mass less than half of that of the Higgs boson.

Although direct detection, indirect detection, and collider search experiments have thus far produced null results for observing DM, they nevertheless are continuing the search with vigor to confirm the conclusion of Clowe et al. [25] of direct empirical proof of the existence of DM. These efforts are largely complimentary as collider searches favor lighter DM masses, indirect detection favors heavier DM masses, and direct detection is optimal for DM masses near heavy nuclear mass ranges. As experimental sensitivities increase and experiments collect more data in the coming years our knowledge of DM will be greatly enhanced, and we may even find a “smoking gun” signatures of dark matter. Potentially we are currently witnessing one the most exciting times in science with the hunt for dark matter.

In this thesis we outline a new class of dark matter scenarios, along with a specific ‘Higgs portal’ implementation, which leads to different predictions for the preferred mass range and coupling strength of dark matter. However, notably, in large parts of parameter space the matter dominated freeze-out scenario we highlight here remains discoverable by these standard searches for dark matter.

Chapter 2

Matter Domination in the Early Universe

This chapter presents original material in Sections 2.2 and 2.3, discussed in [1], and further developed in this thesis.

In this chapter we start by deriving useful relationships between time, scale factor, and temperature. Subsequently, we derive an interpolating version of the Friedmann equation which describes both radiation domination and matter domination in different limits. We then discuss the possible scenarios which can arise for dark matter, before studying these via the interpolating Friedmann equation in the next chapter.

2.1 Relating Time, Scale Factor, and Temperature

Consider the Friedmann-Lemaitre-Robertson-Walker (FLRW) cosmology of a perfect fluid with stress-energy tensor $T_{\nu}^{\mu} = \text{diag}(\rho, -p, -p, -p)$, where $\rho(t)$ is the energy density of the fluid and $p(t)$ is its pressure. Then the 00 component of the Einstein equation gives the Friedmann equation

$$\left(\frac{\dot{a}}{a}\right)^2 + \frac{k}{a^2} = \frac{8\pi G}{3}\rho, \quad (2.1)$$

and *ii* component

$$2\frac{\ddot{a}}{a} + \left(\frac{\dot{a}}{a}\right)^2 + \frac{k}{a^2} = -8\pi Gp, \quad (2.2)$$

where k is the constant parameter of the FLRW metric which determines either a closed ($k = 1$), open ($k = -1$), or flat universe ($k = 0$), and $G = M_{\text{pl}}^{-2}$ is the gravitational constant which may be taken as the inverse of planck mass squared. Subtracting equation (2.1) from (2.2) gives:

$$\frac{\ddot{a}}{a} = -\frac{4\pi G}{3}(\rho + p). \quad (2.3)$$

Moreover, taking the time derivative of equation (2.1),

$$\frac{\ddot{a}}{a} = \frac{4\pi G}{3}\left(\frac{a}{\dot{a}}\dot{\rho} + 2\rho\right), \quad (2.4)$$

and equating to equation (2.3),

$$\frac{\dot{a}}{a} = \frac{\dot{\rho}}{p}. \quad (2.5)$$

For the relationship between energy density and pressure, one must solve for the equation of state. For simplicity, we may take the relationship to be defined by:

$$p = w\rho, \quad (2.6)$$

where w is a constant that is $w = 1/3$ for radiation, $w = 0$ for matter, $w = -1$ for vacuum energy, and $w = -1/3$ for curvature. Substituting equation $p = w\rho$ into eq. (2.5) then integrating we find,

$$\frac{\rho}{\rho_0} = \left(\frac{a}{a_0}\right)^{-3(1+w)} \quad (2.7)$$

Incidentally one could also derive equation (2.7) by invoking the First Law of Thermodynamics, $d(\rho a^3) = -pd(a^3)$, or equivalently, $\partial_\nu T^{0\nu} = 0$.

Substituting equation (2.7) into equation (2.1) gives:

$$\dot{a}^2 = \frac{8\pi G}{3} \rho_0 a_0^{3(1+w)} a^{-(1+3w)} + k. \quad (2.8)$$

For $k = 0$ and $w \neq -1$, integrating equation (2.8) gives:

$$a(t) \propto t^{\frac{2}{3}(1+w)^{-1}} \quad (2.9)$$

and

$$H = \frac{\dot{a}}{a} = \frac{2}{3}(1+w)^{-1}t^{-1}. \quad (2.10)$$

We next derive a useful relation between the FLRW scale factor and temperature, which depends on the equation of state of the universe. Decoupled radiation has the temperature vs scale factor relation $T_{\text{R,decoupled}} \propto a^{-1}$, and decoupled matter has the relation, $T_{\text{M,decoupled}} \propto a^{-2}$. Here we derive the relation between temperature and scale factor for a thermal bath of both matter and radiation. Suppose, for the sake of simplicity, the universe is filled with an ideal gas at temperature T of relativistic ($T \gg m_{\text{R}}$) or non-relativistic particles ($T \ll M_{\text{NR}}$) in thermal equilibrium. Further, label the entropy per particle in this universe \mathcal{S} , the number density of all particles n , and the relativistic and non-relativistic number densities n_{R} and n_{NR} , respectively. Then, by the Second Law of thermodynamics, we have,

$$d\mathcal{S} = \frac{d(\varepsilon/n) + pd(1/n)}{T} \quad (2.11)$$

where,

$$\varepsilon = \varepsilon_{\text{R}} + \varepsilon_{\text{NR}} = 3n_{\text{R}}T + (3/2)n_{\text{NR}}T \quad (2.12)$$

is the energy density, split in relativistic and non-relativistic parts, and

$$p = n_{\text{R}}T + n_{\text{NR}}T \quad (2.13)$$

is the pressure. Since $n = n_{\text{R}} + n_{\text{NR}}$ by assumption, define $y \equiv n_{\text{R}}/n$, so that $1 - y = n_{\text{NR}}/n$. Thus, combining equations (2.11)-(2.13), we have,

$$d\mathcal{S} = \left(\frac{3}{2}\right) \frac{d((1+y)T)}{T} + nd(1/n). \quad (2.14)$$

Integrating,

$$\mathcal{S} = \ln(CT^{(3/2)(1+y)}/n) \quad (2.15)$$

where C is a constant. During equilibrium, $d\mathcal{S} = 0$, and $n \propto a^{-3}$, implying $T^{(3/2)(1+y)}a^3 = \text{const.}$, or $T \propto a^{-2/(1+y)}$. Therefore in the limit that the number density of relativistic particles dominate the total number density, $y \approx 1$ and $T \propto a^{-1}$. In the opposite limit of non-relativistic domination of the number density, $y \approx 0$, and $T \propto a^{-2}$. Letting $\eta \equiv n_{\text{NR}}/n_{\text{R}} = (1 - y)/y$, we can rewrite the above relation as $T \propto a^{-2(1+\eta)/(2+\eta)}$. Today, the number density of baryons to photons is of order 10^{-8} , therefore it is safe to assume that throughout the history of the universe, $\eta \ll 1$, and that the relativistic particles dominate the number density of particles of the universe [38]. We will assume $\eta \ll 1$ throughout this text, hence $T \propto a^{-1}$ during thermal equilibrium.

Additionally, in our universe particles do not stay relativistic, and to a good approximation they become non-relativistic when $T \sim m$. To account for this change, it is common to define a function called the effective entropic degrees of freedom as

$$g_{*S} = \sum_{i=\text{bosons}} g_i \left(\frac{T_i}{T}\right)^3 + \frac{7}{8} \sum_{i=\text{fermions}} g_i \left(\frac{T_i}{T}\right)^3, \quad (2.16)$$

where the sum runs over relativistic particles, and g_i is the degrees of freedom for the i th species [5]. Then the entropy density of the universe can be expressed as follows

$$s = \frac{2\pi^2}{45} g_{*S} T^3. \quad (2.17)$$

Notice that this equation for entropy neglects non-relativistic degrees of freedom, which

is a good approximation in our early universe [5]. Equation (2.17) gives that $g_{*S}a^3T^3 = \text{const.}$, so that, precisely speaking, T does not exactly evolve as a^{-1} when the number of degrees of freedom change. In our work we will take $g_{*S} \approx 107$ throughout any principal period of interest and $T \propto a^{-1}$.

2.2 Interpolating Friedmann Equation

Consider a population of states Φ , either a boson or fermion, with energy density ρ_Φ and suppose at some critical temperature T_\star that ρ_Φ starts to evolve as matter, i.e. it scales as a^{-3} in terms of the FLRW scale factor. The simplest example is the case that Φ is some heavy decoupled species, in which case it become matter-like at $T_\star \sim m_\Phi$ and at temperatures $T > T_\star$ the component of Φ to the energy density is radiation-like, scaling as a^{-4} . It follows that at temperatures below T_\star the Friedmann equation can be expressed as follows¹

$$H^2 = \frac{8\pi}{3M_{\text{pl}}^2} [\rho_R + \rho_\Phi + \rho_X] \simeq \frac{8\pi}{3M_{\text{pl}}^2} \left[\rho_\star r \left(\frac{a_\star}{a}\right)^4 + \rho_\star(1-r) \left(\frac{a_\star}{a}\right)^3 \right] \quad (2.18)$$

where ρ_R and ρ_X are the energy densities of the Standard Model radiation bath and the DM, respectively and we define,

$$\rho_\star \equiv \rho_R + \rho_\Phi|_{T=T_\star} \quad (2.19)$$

and

$$r \equiv \rho_R/(\rho_R + \rho_\Phi)|_{T=T_\star}. \quad (2.20)$$

¹Note the definition of r differs slightly from that in [1], but the two definitions coincide with the assumption that ρ_X is negligible, an assumption which will typically hold.

Thus r represents the fraction of the energy in radiation at temperature T_* and $1 - r$ is the fraction of energy in Φ at $T = T_*$. Equation (2.18) may also be written as

$$H^2 \simeq H_*^2 \left[r \left(\frac{a_*}{a} \right)^4 + (1 - r) \left(\frac{a_*}{a} \right)^3 \right], \quad (2.21)$$

in terms of $H_* \equiv H|_{T=T_*}$ which is given by

$$H_*^2 \equiv \frac{8\pi}{3M_{\text{pl}}^2} \rho_* \equiv \frac{8\pi^3 g_*(T_*)}{90M_{\text{pl}}^2} T_*^4, \quad (2.22)$$

where g_* is the effective number of relativistic degrees of freedom

$$g_* = \sum_{i=\text{bosons}} g_i \left(\frac{T_i}{T} \right)^4 + \frac{7}{8} \sum_{i=\text{fermions}} g_i \left(\frac{T_i}{T} \right)^4 \quad (2.23)$$

which, like the entropic degrees of freedom, the sum runs over relativistic degrees of freedom. We call (2.18) the Interpolating Friedmann equation because it has the limit of matter domination (MD) when $r \rightarrow 0$, and radiation domination (RD) when $r \rightarrow 1$.

While the DM remains coupled to the thermal bath, it has a thermal distribution and the energy density is given as normal by

$$\rho_X = m_X n_X^{EQ}(x) = \begin{cases} m_X \frac{g}{(2\pi)^{3/2}} m_X^3 x^{-3/2} e^{-x} & T \ll m_X \\ \frac{\pi^2}{30} g T^4 & T \gg m_X \end{cases} \quad (2.24)$$

where m_X is the DM mass. During later times DM will undergo freeze-out, but throughout the parameter range relevant to freeze-out, the energy density of DM will be much smaller than that of ρ_* , as we will show in the Chapter 4. Thus we neglect the DM energy density in the Friedmann Equation, to aid in calculating freeze-out abundances.

2.3 Early Universe Scenarios with a Matter-like Species

Although precise definitions and derivations for terms used in this section will be shown in subsequent chapters, here we give a broad overview of the richer range of scenarios that the inclusion of the matter-like state Φ offers. Which scenario is realized depends on the ordering of the freeze-out temperature T_F , the temperature at which matter dominates the energy density T_{MD} , and the temperature of the bath at the point of Φ decays $T_\Gamma \equiv T(t \sim \Gamma_\Phi^{-1})$:

- i). *Radiation Domination*: If Φ decays prior to DM freeze-out $T_\Gamma \gg T_F$, then DM decouples during radiation domination with $H \propto T^2$ and there is no period of Φ matter domination.
- ii). *Radiation Domination with dilution*: DM decouples during radiation domination, again $H \propto T^2$, but Φ later evolves to dominate the energy density. Decays of Φ dilute or repopulate the DM freeze-out abundance [39]. In this case DM decouples prior to both matter domination and Φ decays: $T_F \gg T_\Gamma, T_{\text{MD}}$.
- iii). *Matter Domination*: DM decouples while Φ is matter-like and dominates the energy density of the universe, at which point $H \propto T^{3/2}$ assuming adiabicity. This scenario is realized for $T_{\text{MD}} \gg T_F \gg T_\Gamma$.

It is also important to compare these quantities to the reheat temperature after Φ decays² $T_{\text{RH}} \simeq \sqrt{M_{\text{Pl}}\Gamma_\Phi}$. If one treats Φ decays as instantaneous, it appears that there is a discontinuous jump in the bath temperature from T_Γ to T_{RH} . This is an artifact of the sudden decay approximation. Using instead an exponential decay law this jump is absent, rather there is a smooth interpolation and the temperature never rises at any stage [40]. The effect of Φ decays is seen as a reduction in the rate of cooling.

²We use T_{RH} throughout to refer to the heating associated to Φ decays (rather than inflationary reheating).

For processes around $T \sim T_{\text{RH}}$ the impact of non-instantaneous Φ decays must be taken into account. Specifically, for DM decoupling with $T_F \sim T_{\text{RH}}$, the Boltzmann equations must be modified to include contributions to the number densities due to Φ decays, similar to [6, 7]. However, for processes active at temperatures away from this period, instantaneous decay is a fine approximation. In Chapter 5 we discuss the case in which there is not a clear separation between the times of freeze-out and reheating due to Φ decay, i.e. $T_F \sim T_{\text{RH}}$.

While scenarios (i) & (ii) have been discussed in the literature, to our knowledge, case (iii) remains largely unstudied. However, matter dominated freeze-out is a very general possibility which readily reproduces the DM relic density and thus we dedicate this thesis to the thorough study of case (iii).

We note here that the prospect of matter dominated freeze-out was remarked upon briefly in other contexts in [41, 42]. Moreover, this scenario is also similar in spirit to [6, 43, 44] which studied DM freeze-out during inflationary reheating, in which case $H \propto T^4$. Matter-dominated Freeze-out differs from these in several ways, most significantly, these other works consider the case in which the radiation bath is initially negligible. Here, rather, we assume the Φ states decay at times well after inflationary reheating, when there is a well established thermal bath, and that DM freeze-out occur significantly after inflationary reheating and while Φ decays are entirely negligible, thus preserving adiabaticity.

Interestingly, the impact of an early period of matter domination on DM has been considered from different perspectives in recent papers, e.g. [39, 42, 45–47]. Also, an interesting variant, not captured in our list (i)-(iii), is if DM freeze-out occurs while the universe is dominated by an energy density redshifting faster than radiation [48], one example is kinetic energy (‘kination’) dominated, e.g. [49, 50].

Chapter 3

Freeze-out of Dark Matter

During Matter Domination

This chapter presents some of the main original results of this thesis: eqns. (3.10), (3.34) & (3.40) This has been discussed in [1], and is further developed in this thesis.

If DM freeze-out occurs while the universe is dominated by an energy density which redshifts as matter-like, this changes the expansion rate of the universe H and thus will impact the freeze-out dynamics. In this chapter we will study matter dominated freeze-out (MDFO) of DM in a model independent manner, highlighting the major differences with conventional radiation dominated freeze-out (RDFO). Notably, we observed that the decay of the matter-like field which leads to the early period of matter domination can dilute the DM, thus allowing for smaller annihilation cross section or much heavier DM, while evading experimental searches. In subsequent chapters I will broadly identify the range of viable parameter space and study this intriguing possibility in the context of Higgs portal DM.

We begin by explaining the freeze-out process and deriving an interpolating freeze-out temperature formula which has MD and RD limits in the first section. We then move to studying the Boltzmann equation and putting in a from conducive to cosmological

studies. This will then allow us to calculate an interpolating abundance of DM in the third section, and the fourth section will use the abundance to present the relic density of DM in light of entropy injections. The final section of this chapter will be used to derive an equation for the dilution factor that quantifies entropy injections in terms of reheating.

3.1 Freeze-out Temperature

First we calculate the freeze-out temperature. Freeze-out is the process that a particle species of the universe undergoes through which the creation and annihilation processes of such a species become decisively rare, thus rendering the number of particles of such a species effectively constant. Consider an interaction of the form, $\Gamma \propto T^\gamma$, and Hubble parameter $-\dot{T}/T = H \propto T^\eta$. Then the number of interactions after comoving time t is:

$$N_{int} = \int_t^\infty dt' \Gamma(t') = \left(\frac{\Gamma}{H} \right) \Big|_T T^{-(\gamma-\eta)} \int_0^T dT' (T')^{\gamma-\eta-1} = \left(\frac{\Gamma}{H} \right) \Big|_T \frac{1}{(\gamma-\eta)}. \quad (3.1)$$

Assuming $\gamma - \eta > 1$, equation (3.1) shows that less than one interaction is likely after the temperature drops below the temperature at which $\Gamma = H$. Therefore we define the freeze-out temperature, $T_F \equiv m_X x_F^{-1}$ implicitly using the condition:

$$\Gamma(x_F) \equiv H(x_F). \quad (3.2)$$

We will take the annihilation interaction rate for the dark matter candidate to be,

$$\Gamma_{ann} = n_X^{\text{EQ}} \langle \sigma_A |\vec{v}| \rangle, \quad (3.3)$$

where,

$$n_X^{\text{EQ}}(x) = \frac{g}{(2\pi)^{3/2}} m_X^3 x^{-3/2} e^{-x}, \quad (3.4)$$

and the thermally average annihilation cross-section is parameterized as,

$$\langle \sigma_A |\vec{v}| \rangle \equiv \sigma_0 x^{-n} \quad (3.5)$$

Moreover we define $x_\star \equiv m_X/T_\star$. Then, neglecting the small dark matter contribution and using the relation $T/T_\star = a_\star/a$, the Friedmann equation (2.21) may be re-written as:

$$H = H_\star \sqrt{1-r} \left(\frac{x_\star}{x} \right)^{3/2} \left[\frac{r}{1-r} \left(\frac{x_\star}{x} \right) + 1 \right]^{1/2} \quad (3.6)$$

Using equations (3.3)-(3.6) in definition (3.2), we find x_F to be

$$x_F = \ln \left[\frac{gm_X^3 \sigma_0}{(2\pi)^{3/2} H_\star x_\star^{3/2}} (1-r)^{-1/2} \left(x_F^{2n} + \frac{rx_\star}{1-r} x_F^{-1+2n} \right)^{-1/2} \right] \quad (3.7)$$

Equation (3.7) can be solved numerically, but is highly insensitive to the parameter space we consider. Therefore we may approximate it iteratively, by initially guessing $x_F^{(0)} = 1$ on the RHS, and getting that the LHS is

$$x_F^{(1)} \approx \ln \left[\frac{gm_X^3 \sigma_0}{(2\pi)^{3/2} H_\star x_\star^{3/2}} (1-r)^{-1/2} \left(1 + \frac{rx_\star}{1-r} \right)^{-1/2} \right] \quad (3.8)$$

By taking the $r \rightarrow 1$ and $r \rightarrow 0$ limits of equation (3.8) we obtain the RD and MD limits, respectively:

$$(x_F^{\text{RD}})^{(1)} \equiv \lim_{r \rightarrow 1} x_F^{(1)} = \ln \left[\frac{gm_X^3 \sigma_0}{(2\pi)^{3/2} H_\star x_\star^2} \right] = \ln \left[\frac{3}{4\pi^3} \sqrt{\frac{5}{2}} \frac{g}{\sqrt{g_\star(T_\star)}} m_X M_{\text{pl}} \sigma_0 \right], \quad (3.9)$$

and

$$(x_F^{\text{MD}})^{(1)} \equiv \lim_{r \rightarrow 0} x_F^{(1)} = \ln \left[\frac{gm_X^3 \sigma_0}{(2\pi)^{3/2} H_\star x_\star^{3/2}} \right] = \ln \left[\frac{3}{4\pi^3} \sqrt{\frac{5}{2}} \frac{g}{\sqrt{g_\star(T_\star)}} \frac{m_X^{3/2} M_{\text{pl}} \sigma_0}{\sqrt{T_\star}} \right] \quad (3.10)$$

The numerical solution to equation (3.7), using $n = 0$ (the only case we consider in this work), with $m_X = T_\star = \sigma_0^{-1/2} = 10^2$ GeV and $r \approx 0$ (MD), is $x_F = 34.4$. Using the weak scale again, but with $r \approx 1$ (RD) yields $x_F = 36.2$. Using the same equation, but with $n = 0$, $m_X = T_\star = \sigma_0^{-1/2} = 10^9$ GeV and $r \approx 0$ gives $x_F = 18.3$. Using the 10^9 GeV scale but with $r \approx 1$ gives $x_F = 19.81$.

Had we used the approximations in eqns. (3.9) and (3.10), the only significant difference would be for the case of RD, with $(x_F^{\text{RD}})^{(1)} \approx 34.4$ rather than the 36.2 above in the weak scale, and $(x_F^{\text{RD}})^{(1)} \approx 18.3$ rather than 19.8 above in the 10^9 GeV scale. In summary, the approximation eqns. (3.9) and (3.10) are in excellent agreement with the exact results in the MD case, and only differs by $\sim 5\%$ in the RD case. Moreover, using the approximation eqns. (3.9) and (3.10) yields very little change between the RD and MD cases (they agree exactly up to the significant digits we used), while the MD and RD case differ by the same $\sim 5\%$ in the exact numerical solution of eq. (3.7).

Because there is little change in the values of x_F throughout the wide range of parametrics we consider, we will take the characteristic x_F of the Weak scale to be $x_F^{\text{char,weak}} \simeq 35$, and in the 10^9 GeV scale to be, $x_F^{\text{char},10^9\text{GeV}} \simeq 19$. Moreover, to ensure a finite freeze-out temperature when using approximation (3.10), in the case of MD we need that $x_F^{\text{MD}} > 0$ or, equivalently,

$$T_\star \lesssim \frac{45}{32\pi^6} \frac{g^2}{g_*(T_\star)} m_X^3 M_{\text{pl}}^2 \sigma_0^2. \quad (3.11)$$

For an upper bound on x_\star in the case of MD we must ensure that $x_\star \leq x_F$ so that the freeze-out temperature is lower than the critical temperature. Although this condition cannot be written analytically, solving it iteratively gives a rough upper bound to x_\star as

$$x_\star \lesssim \ln \left[\frac{3}{4\pi^3} \sqrt{\frac{5}{2}} \frac{g}{\sqrt{g_*(T_\star)}} m_X M_{\text{pl}} \sigma_0 \right]. \quad (3.12)$$

More stringent constraints will be derived in the Constraints segment of this work.

3.2 The Boltzmann Equation

In cosmology the Boltzmann Equation is used to describe the change in the phase space distribution, and consequently the number density, of a species in scenarios beyond thermal equilibrium. The relativistic Boltzmann Equation is

$$\hat{\mathbf{L}}[f] = \mathbf{C}[f], \quad (3.13)$$

where f is the phase space distribution function, \mathbf{C} is the collision operator, and $\hat{\mathbf{L}}$ is the relativistic Liouville operator:

$$\hat{\mathbf{L}} = p^\alpha \partial_\alpha - \Gamma_{\beta\gamma}^\alpha p^\beta p^\gamma \frac{\partial}{\partial p^\alpha}. \quad (3.14)$$

Since the FLRW cosmology is homogeneous and isotropic, $f = f(E, t)$ if follow that

$$\hat{\mathbf{L}}[f(E, t)] = E \frac{\partial f}{\partial t} - \frac{\dot{a}}{a} |\vec{p}|^2 \frac{\partial f}{\partial E} = \mathbf{C}[f]. \quad (3.15)$$

Multiplying the LHS of eq. (3.15) by $g/((2\pi)^3 E)$ and integrating gives

$$\frac{g}{(2\pi)^3} \int \frac{d^3 p}{E} \hat{\mathbf{L}}[f] = \frac{g}{(2\pi)^3} \int d^3 p \frac{\partial f}{\partial t} - \frac{g}{(2\pi)^3} \int \frac{d^3 p}{E} \frac{\dot{a}}{a} |\vec{p}|^2 \frac{\partial f}{\partial E}. \quad (3.16)$$

The first term on the RHS of equation (3.16) is just $\frac{\partial}{\partial t} \frac{g}{(2\pi)^3} \int d^3 p f = \frac{\partial n}{\partial t}$, where n is the number density. For the second term on the RHS of equation (3.16) we will integrate by parts and use the relation $E dE = p dp$:

$$-\frac{g}{(2\pi)^3} \int \frac{d^3 p}{E} \frac{\dot{a}}{a} |\vec{p}|^2 \frac{\partial f}{\partial E} = \frac{-Hg(4\pi)}{(2\pi)^3} \int \frac{dpp}{E} p^3 \frac{\partial f}{\partial E} = \frac{Hg(4\pi)}{(2\pi)^3} \int dE \frac{\partial p^3}{\partial E} f. \quad (3.17)$$

Taking the derivative of p^3 and using $E dE = p dp$ again:

$$\frac{3Hg(4\pi)}{(2\pi)^3} \int dE E p f = 3H \frac{g}{(2\pi)^3} \int d^3 p f = 3H n. \quad (3.18)$$

Therefore the Boltzmann equation becomes

$$\dot{n} + 3Hn = \frac{g}{(2\pi)^3} \int \frac{d^3p}{E} \mathbf{C}[f]. \quad (3.19)$$

Focusing on the collision term, and considering the Boltzmann equation for a species X , the collision term for the most general process $X + a + b + \dots \longleftrightarrow i + j + \dots$ may be written as

$$\begin{aligned} \frac{g}{(2\pi)^3} \int \frac{d^3p}{E} \mathbf{C}[f] = & - \int d\Pi_X d\Pi_a d\Pi_b \dots d\Pi_i d\Pi_j \dots \\ & \times (2\pi)^4 \delta^4(p_X + p_a + p_b \dots - p_i - p_j \dots) \\ & \times [|\mathcal{M}|_{X+a+b+\dots \rightarrow i+j+\dots}^2 f_a f_b \dots f_X (1 \pm f_i)(1 \pm f_j) \dots] \\ & - |\mathcal{M}|_{i+j+\dots \rightarrow X+a+b+\dots}^2 f_i f_j \dots (1 \pm f_a)(1 \pm f_b) \dots (1 \pm f_X)] \quad (3.20) \end{aligned}$$

where the various f_s are phase space densities for their respective species s ; (+) or (−) in the $(1 \pm f_s)$ are used for bosons and fermions, respectively; finally, for g internal degrees of freedom:

$$d\Pi \equiv g \frac{1}{(2\pi)^3} \frac{d^3p}{2E}. \quad (3.21)$$

Following [5] we will make a series of reasonable assumptions to simplify the collision part of the Boltzmann equation. The first is T -symmetry in any interactions. The second is the use of Maxwell-Boltzmann (MB) statistics, thus we ignore the emission factors $1 \pm f_s \approx 1$, where for MB statistics, $f_s = \exp[-(E_s - \mu_s)/T]$. The third assumption is that any dark matter candidate we consider will be stable relative to the age of the universe, so that decaying dark matter will not be considered. The fourth assumption is C -symmetry, so that we treat dark matter particles and anti-particles on the same footing, and with the same abundances. The fifth assumption is that the chemical potentials of the annihilation products are zero, as well as the initial chemical potential of the

dark matter species (though the DM chemical potential changes when the temperature of the bath drops well below its mass [51]). The sixth assumption is that the dark matter candidate is in *kinetic*¹ equilibrium with the rest of the thermal bath, sharing the temperature of photons and keeping a MB thermal distribution. Making all these assumptions, the Boltzmann equation can be written as

$$\dot{n} + 3Hn = -\langle\sigma_{\text{A}}|\vec{v}|\rangle[n^2 - (n^{\text{EQ}})^2], \quad (3.22)$$

where $\langle\sigma_{\text{A}}|\vec{v}|\rangle$ is the thermally-averaged annihilation cross-section.

To mod out the change in number density due to expansion we define the dimensionless $Y \equiv n/s$, termed abundance. Moreover, define $x \equiv m_X/T$ so that we may consider only dimensionless parameters. When the entropy per comoving volume is conserved it follows that

$$\dot{n} + 3Hn = s\dot{Y} = s\frac{dY}{dx}\frac{dx}{dt}. \quad (3.23)$$

We thus finally arrive at the standard BE used for cosmological studies

$$\frac{dY}{dx} = -\left(\frac{dt}{dx}\right)\frac{\langle\sigma_{\text{A}}|\vec{v}|\rangle}{s}[n^2 - (n^{\text{EQ}})^2] = -\left(\frac{dt}{dx}\right)\langle\sigma_{\text{A}}|\vec{v}|\rangle s[Y^2 - Y_{\text{EQ}}^2]. \quad (3.24)$$

3.3 Freeze-out Abundance

Next we wish to calculate the freeze-out abundance. Let $\Delta \equiv Y - Y_{\text{EQ}}$, then equation (3.24), using equations (2.17) and (3.5), may be written:

$$\Delta' = -Y'_{\text{EQ}} - \left(\frac{dt}{dx}\right)\sigma_0 x^{-n} \left(\frac{2\pi^2}{45}g_{*S}m_X^3 x^{-3}\right)\Delta[2Y_{\text{EQ}} + \Delta]. \quad (3.25)$$

¹It is possible to maintain a MB thermal distribution for DM at the temperature of the bath, termed kinetic equilibrium, while not maintaining an equilibrium balance of chemical potentials, termed chemical equilibrium [51].

Furthermore, for the $\frac{dt}{dx}$ relation, we use that $a \propto T^{-1}$ (hence $H = -\dot{T}/T$) to arrive at

$$\frac{dx}{dt} = \frac{m_X}{T} \left(\frac{-\dot{T}}{T} \right) = xH. \quad (3.26)$$

From equations (3.25) and (3.26) we have

$$\Delta' = -Y'_{\text{EQ}} - \left[\frac{2\pi^2 g_{*S} m_X^3 \sigma_0}{45 H_* x_*^{3/2}} \right] (1-r)^{-1/2} \left(1 + \frac{r}{(1-r)} \frac{x_*}{x} \right)^{-1/2} x^{-5/2-n} \Delta [2Y_{\text{EQ}} + \Delta], \quad (3.27)$$

where primes stand for derivative with respect to x . Define,

$$\lambda \equiv \frac{2\pi^2 g_{*S} m_X^3 \sigma_0}{45 H_* x_*^{3/2}} = \frac{\sqrt{\pi}}{3\sqrt{5}} \frac{g_{*S}}{\sqrt{g_*(T_*)}} \frac{M_{\text{pl}} m_X^{3/2} \sigma_0}{\sqrt{T_*}}. \quad (3.28)$$

Since we are interested the freeze-out abundance we consider primarily the domain $x \gg x_F$. In this regime we have $Y \gg Y_{\text{EQ}}$, so that $\Delta \approx Y$. We may also neglect Y'_{EQ} in the late time regime. Then equation (3.27) approximates to

$$\Delta' \approx -\lambda (1-r)^{-1/2} \left(1 + \frac{r}{(1-r)} \frac{x_*}{x} \right)^{-1/2} x^{-5/2-n} \Delta^2 \quad (3.29)$$

Integrating equation (3.29), we arrive at $Y(x \rightarrow \infty) \equiv Y_\infty$

$$Y_\infty \approx \Delta_\infty \approx \left[\lambda (1-r)^{-1/2} \int_{x_F}^{\infty} dx \left(1 + \frac{r}{(1-r)} \frac{x_*}{x} \right)^{-1/2} x^{-5/2-n} \right]^{-1}. \quad (3.30)$$

Note that we used $Y_\infty \ll Y_{x_F}$, in arriving at equation (3.30). The integral on the RHS of equation (3.30) is not particularly useful in its present form, with Mathematica finding,

$$\int_{x_F}^{\infty} dx \left(1 + \frac{r}{(1-r)} \frac{x_*}{x} \right)^{-1/2} x^{-5/2-n} = \left(\frac{-r x_*}{1-r} \right)^{-3/2-n} B(-r x_*/(1-r) x_F; 3/2+n, 1/2), \quad (3.31)$$

where $B(\cdot; \cdot, \cdot)$ is the Incomplete Beta function. A more enlightening form comes when $n = 0$,

$$\begin{aligned} & \int_{x_F}^{\infty} dx \left(1 + \frac{r}{(1-r)} \frac{x_{\star}}{x} \right)^{-1/2} x^{-5/2} \\ &= \frac{(1-r)}{rx_{\star}x_F} \left(\sqrt{x_F + rx_{\star}/(1-r)} - x_F \sqrt{(1-r)/rx_{\star}} \operatorname{arcsinh} \sqrt{rx_{\star}/(1-r)x_F} \right). \end{aligned} \quad (3.32)$$

To see the behavior of Y_{∞} in the limits of RD and MD, consider first the standard radiation dominated case (as in [52])

$$Y_{\infty}^{\text{RD}} \equiv \lim_{r \rightarrow 1} Y_{\infty} = \frac{\sqrt{x_{\star}}}{\lambda} (n+1) x_F^{n+1} = 3 \sqrt{\frac{5}{\pi}} \frac{\sqrt{g_{\star}(T_{\star})}}{g_{\star S}(T_F)} \frac{(n+1) x_F^{n+1}}{M_{\text{pl}} m_X \sigma_0}. \quad (3.33)$$

Finally for the freeze-out abundance in the MD case we have

$$Y_{\infty}^{\text{MD}} \equiv \lim_{r \rightarrow 0} Y_{\infty} = \frac{1}{\lambda} (n+3/2) x_F^{n+3/2} = 3 \sqrt{\frac{5}{\pi}} \frac{\sqrt{g_{\star}(T_{\star})}}{g_{\star S}(T_F)} \frac{(n+3/2) x_F^{n+3/2}}{M_{\text{pl}} m_X \sigma_0 \sqrt{x_{\star}}}. \quad (3.34)$$

One immediate difference is that $Y_{\infty}^{\text{MD}} \propto (x_F^{\text{MD}})^{n+3/2}$, whereas in the radiation dominated case $Y_{\infty}^{\text{RD}} \propto (x_F^{\text{RD}})^{n+1}$. Another notable difference is that Y_{∞}^{MD} has a new parameter dependence, namely varying with the quantity x_{\star} .

3.4 Dark Matter Relic Density

Even if freeze-out occurred during MD, to recover the successful Big Bang Nucleosynthesis (BBN) paradigm RD must be restored at its onset. This is possible through the decay of a massive particle species or coherent oscillations of a scalar field, thus injecting a large amount of entropy dominated by light degrees of freedom [39].

Not only do entropy injections ensure RD at the inception of BBN, but they may also considerably increase the parameter space. Suppose there is an instant decay of a massive particle species (or an instantaneously decaying coherently oscillating scalar

field), such that the products of this decay are relativistic and do not repopulate the candidate DM species (the exact parametrics for ensuring this scenario will be discussed in the Constraints segment of this work). Then the number density of candidate DM stays fixed, while the entropy density increases by the inverse of

$$\zeta \equiv s_{\text{before}}/s_{\text{after}}. \quad (3.35)$$

Then, the relic abundance relative to the computed freeze-out abundance above (label it Y_{∞}^F for this section) is

$$Y_{\infty}^{\text{relic}} = n_X/s_{\text{after}} = \zeta n_X/s_{\text{before}} = \zeta Y_{\infty}^F. \quad (3.36)$$

The DM abundance Y can be re-expressed in terms of

$$\Omega_X h^2 = s_0 m_X Y_{\infty}^{\text{relic}} / \rho_{\text{critical}}, \quad (3.37)$$

by scaling with the critical density $\rho_{\text{critical}} \simeq 8.13 \times 10^{-47} \text{GeV}^4$ and the entropy density today $s_0 \simeq 2.29 \times 10^{-38} \text{GeV}^3$. Consequently, this changes the relic density by a factor ζ ,

$$\Omega_X^{\text{relic}} h^2 = \zeta \Omega_X^F h^2. \quad (3.38)$$

Thus with an entropy injection following radiation or matter dominated freeze-out, the final abundance of dark matter can be drastically altered via the dilution factor

$$(\Omega_X^{\text{RD}})^{\text{relic}} h^2 \sim 0.1 \cdot \left(\frac{m_X}{10^6 \text{GeV}} \right)^2 \left(\frac{0.1}{\alpha} \right)^2 \left(\frac{\zeta}{10^{-5}} \right), \quad (3.39)$$

$$(\Omega_X^{\text{MD}})^{\text{relic}} h^2 \sim 0.1 \cdot \left(\frac{m_X}{10^6 \text{GeV}} \right)^2 \left(\frac{0.1}{\alpha} \right)^2 \left(\frac{10^2}{x_{\star}} \right)^{1/2} \left(\frac{\zeta}{10^{-5}} \right). \quad (3.40)$$

where we parameterized $\sigma_0 = \alpha^2/m_X^2$, set $g_{\star} \sim g_{\star S} \simeq 107$, $n = 0$, and fixed x_F to a characteristic value of 27. Figures 3.1 and 3.2 show the MD parametrics.

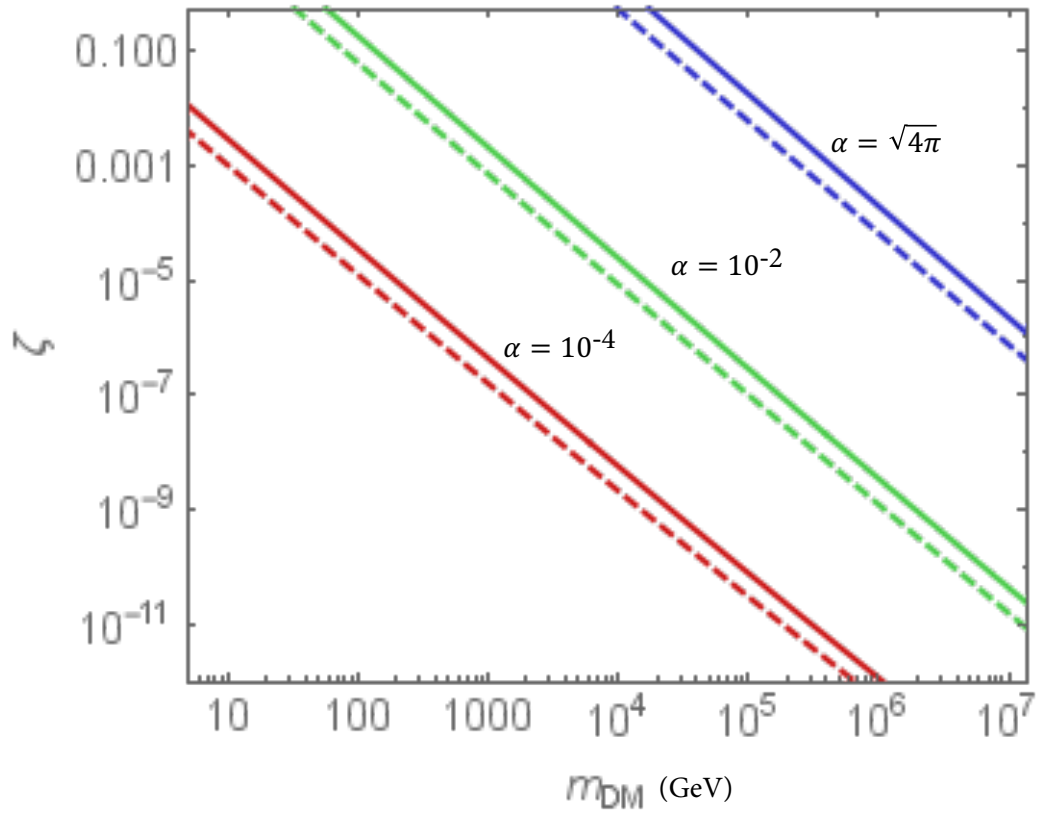


Figure 3.1: m_X vs ζ plot in MD FO case for $\alpha = \sqrt{4\pi}$ (blue); $\alpha = 10^{-2}$ (green); and $\alpha = 10^{-4}$ (red). The dashed lines are for $x_\star = 1$ and solid lines, $x_\star = 10$. The dilution factor ζ allows for much heavier DM, given the above coupling strengths, in order to match the CDM relic density observed today.

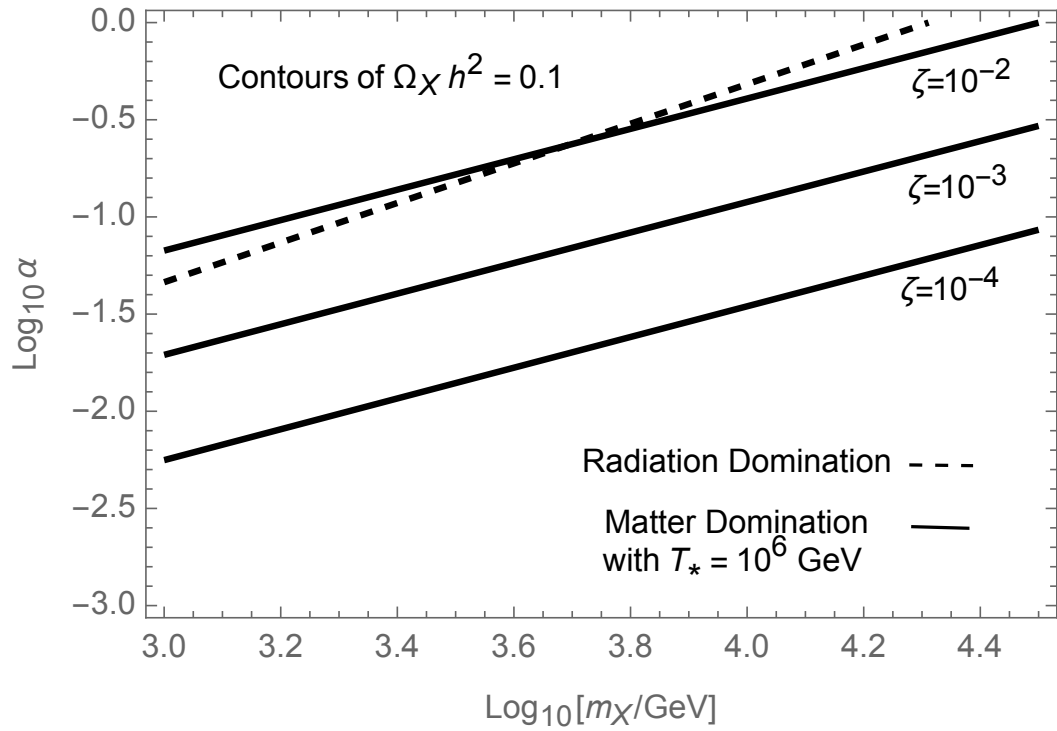


Figure 3.2: Contours of $\Omega_\chi h^2 = 0.1$ for matter (solid) and radiation (dashed) dominated freeze-out scenarios as we vary DM mass and coupling α . Matter domination has two extra parameter freedoms, we fix $T_* = 10^6 \text{ GeV}$ and vary ζ .

3.5 The Dilution Factor

We next derive specific relations for the ζ parameter discussed above. To find an expressions for ζ we derive expressions for $T_\Gamma \equiv T(H = \Gamma)$ and the reheat temperature T_{RH} , being the temperature of the decay products of Φ assuming instantaneous reheating.

Decay of the Φ matter occurs when $H \equiv \Gamma$. Subscripts of Γ represent the value of the corresponding parameter at the time of decay. The scale factor at the time of decay may be obtained by solving the Friedmann equation when $H = \Gamma$. To obtain a solution, change variables in the Friedmann equation using the transformation,

$$\bar{f}_\Phi \equiv \frac{(1-r)}{r} \left(\frac{a}{a_\star} \right), \quad (3.41)$$

so that the Friedman equation can be written as,

$$\xi \bar{f}_\Phi^4 - \bar{f}_\Phi - 1 = 0, \quad (3.42)$$

where

$$\xi \equiv \left(\frac{\Gamma}{H_\star} \right)^2 \frac{r^3}{(1-r)^4}, \quad (3.43)$$

The only real and positive solution is, in exact form,

$$\left(\frac{a_\star}{a} \right)_\Gamma^{-1} = \frac{r}{1-r} \frac{1}{2(6)^{1/3} \sqrt{\xi} q^{1/6}} \left[\sqrt{p} + \left(8(3)^{1/3} \xi - 2^{1/3} q^{2/3} + 12 \sqrt{\frac{\xi q}{p}} \right)^{1/2} \right] \quad (3.44)$$

where,

$$\begin{aligned} q &\equiv 9\xi + \sqrt{3}\xi \sqrt{27 + 256\xi}, \\ p &\equiv -8(3)^{1/3} \xi + 2^{1/3} q^{2/3} \end{aligned} \quad (3.45)$$

Equation (3.44) has simpler expressions in the extreme limits of r , but also when the Friedmann equation is dominated by the matter component. The latter condition places the constraint that Γ is sufficiently small relative to H so that matter will come to

dominate before decay. Thus, we may expand equation (3.44) in powers of Γ/H_\star around zero. Doing so we obtain the approximation,

$$\left(\frac{a_\star}{a}\right)_\Gamma \approx \frac{1}{(1-r)^{1/3}} \left(\frac{\Gamma}{H_\star}\right)^{2/3} - \frac{1}{3} \frac{r}{(1-r)^{5/3}} \left(\frac{\Gamma}{H_\star}\right)^{4/3} + \mathcal{O}\left(\left(\frac{\Gamma}{H_\star}\right)^{8/3}\right) \quad (3.46)$$

Moreover, when $r \ll 1$, we may expand equation (3.44) in powers of r thusly

$$\left(\frac{a_\star}{a}\right)_\Gamma \approx \left(\frac{\Gamma}{H_\star}\right)^{2/3} + \frac{1}{3}r \left(\frac{\Gamma}{H_\star}\right)^{2/3} + \mathcal{O}(r^2). \quad (3.47)$$

Notice that $(1-r)^{-1/3} \approx 1 + r/3 + \mathcal{O}(r^2)$, so that both expansions above approximately agree to first order terms. Finally, since $T/T_\star = a_\star/a$, the temperature of the thermal bath at decay is,

$$T_\Gamma = T_\star \left(\frac{a_\star}{a}\right)_\Gamma. \quad (3.48)$$

We will assume the Φ matter decays to radiation instantaneously, then the temperature of the decay products is

$$T_{\text{RH}} \equiv \left(\frac{30}{\pi^2 g_*(T_{\text{RH}})} \rho_\Phi|_{t \sim \Gamma^{-1}}\right)^{1/4} = \left(\frac{30}{\pi^2 g_*(T_{\text{RH}})} (1-r) \rho_\star \left(\frac{a_\star}{a}\right)_\Gamma^3\right)^{1/4}. \quad (3.49)$$

This equation can be further simplified,

$$T_{\text{RH}} = \left((1-r) \hat{\gamma} \left(\frac{a_\star}{a}\right)_\Gamma^3\right)^{1/4} T_\star, \quad (3.50)$$

where,

$$\hat{\gamma} \equiv \frac{g_*(T_\star)}{g_*(T_{\text{RH}})}. \quad (3.51)$$

This radiation energy subsequently thermalizes instantaneously with the radiation present right before decay. We will generally be interested in the case in which radiation from decay is much larger than the radiation present before decay.

Given the expressions for T_{RH} and T_{Γ} the dilution parameter ζ can be expressed

$$\zeta \equiv \frac{s_{\text{before}}}{s_{\text{after}}} = \frac{[s_R]_{\text{before}}}{[s_{\text{RH}}]_{\text{after}}} = \frac{\frac{2\pi^2}{45} g_{*S}(T_{\Gamma}) T_{\Gamma}^3}{\frac{2\pi^2}{45} g_{*S}(T_{\text{RH}}) T_{\text{RH}}^3}, \quad (3.52)$$

where,

$$s_{\text{RH}} \equiv \frac{2\pi^2}{45} g_{*S}(T_{\text{RH}}) T_{\text{RH}}^3, \quad (3.53)$$

is the entropy in the Reheat radiation after decay and thermalization. Simplifying equation (3.52) we obtain,

$$\zeta = \left(\frac{g_{*S}(T_{\Gamma})}{g_{*S}(T_{\text{RH}})} \right) \left(\frac{T_{\Gamma}}{T_{\text{RH}}} \right)^3. \quad (3.54)$$

Finally, for $\Gamma/H_{\star} \ll 1$ so that we use only the first term of approximation (3.46), we have,

$$\zeta \approx \frac{g_{*}(T_{\Gamma})/g_{*}(T_{\star})}{(1-r)} \frac{T_{\text{RH}}}{T_{\star}}, \quad (3.55)$$

where we have used $g_{*} \approx g_{*S}$ and the following relationship that is a consequence of $\Gamma/H_{\star} \ll 1$:

$$\Gamma \approx \frac{H_{\star}}{\sqrt{\tilde{\gamma}} T_{\star}^2} T_{\text{RH}}^2. \quad (3.56)$$

It follows that ζ is parametrically

$$\zeta \sim 10^{-5} \times \left(\frac{0.1}{1-r} \right) \left(\frac{T_{\text{RH}}}{1 \text{ GeV}} \right) \left(\frac{10^8 \text{ GeV}}{T_{\star}} \right). \quad (3.57)$$

Thus although the parameter ζ , critical for setting the DM relic density, can take a wide range of values, it is not unbounded. Indeed, there are several consistency conditions and constraints which must be satisfied for matter dominated DM freeze-out to be viable. Note that in all cases of interest we have that $T_{\star} \gg T_{\text{RH}}, T_{\text{FO}}, T_{\Gamma}$. In the next chapter we will explore the wider range of theoretical and experimental constraints on this scenario.

Chapter 4

Constraints on Matter Dominated Freeze-out

This chapter presents original results which have been discussed briefly in [1], but is significantly expanded upon in this thesis.

In this chapter we enumerate the constraints on the Matter Dominated Freeze-out scenario. The following constraints provide the strongest model independent bounds on the parameter space:

1. Freeze-out of dark matter before decay of Φ matter.
2. Freeze-out of dark matter during matter domination.
3. Sufficiently high reheat temperature from Φ Decays.

In addition to the above, as we discuss in Section 4.4, the following requirements follow from our assumption on the ordering of scales that $T_{\text{MD}} \gg T_{\text{FO}} \gg T_{\Gamma}$, namely

- 4a. Decay of Φ matter occurs below T_{\star} and T_{MD} .
- 4b. Freeze-out temperature of dark matter is finite and less than T_{\star} and T_{MD} .
- 4c. The reheat temperature does not exceed T_{\star} and T_{MD} .

We consider each of these constraints in the subsections which follow and in Section 4.5 we provide a summary of the leading constraints and an illustrative example of the viable parameter space for such models. We also require that decays of Φ are negligible during freeze-out, essentially that $T_{\text{RH}} \ll T_{\text{FO}}$, but we reserve a careful discussion of this requirement for the next chapter.

4.1 Freeze-out of dark matter during matter domination

For this section we need a precise definition of what we mean by “matter domination”. In [39] the authors define matter domination as the state of the universe when matter constitutes at least half of the energy density of the universe. Here we take a more general approach that is able to recover the definition of the authors of [39]. The definition we take of “matter domination” is as follows: Matter domination is the state of a universe constituted primarily of matter and radiation when the Hubble parameter is sufficiently small relative to a characteristic Hubble parameter scale such that any matter component of the universe constitutes the principal, and to a *fair approximation* the only, contributor to the dynamics of the Friedmann Equation. Mathematically, we have from the Friedmann equation that when $H/H_\star \ll 1$,

$$\left(\frac{a_\star}{a}\right) \approx \frac{1}{(1-r)^{1/3}} \left(\frac{H}{H_\star}\right)^{2/3} - \frac{1}{3} \frac{r}{(1-r)^{5/3}} \left(\frac{H}{H_\star}\right)^{4/3} + \mathcal{O}\left(\left(\frac{H}{H_\star}\right)^{8/3}\right). \quad (4.1)$$

To reasonable approximation matter is the only contributor to the dynamics of the Friedmann equation when the second term in equation (4.1) is much smaller than the first. The exact relation between the first two terms may be parameterized by using a factor β , implicitly defined along with H_{MD} as,

$$\frac{\beta}{(1-r)^{1/3}} \left(\frac{H_{\text{MD}}}{H_\star}\right)^{2/3} \equiv \frac{1}{3} \frac{r}{(1-r)^{5/3}} \left(\frac{H_{\text{MD}}}{H_\star}\right)^{4/3} \quad (4.2)$$

Thus, H_{MD} is the Hubble parameter below which the regime of matter domination ensues, and it is such that the second term of equation (4.1) is a factor β smaller than the first. Equation (4.1) may be solved explicitly for H_{MD} as,

$$\frac{H_{\text{MD}}}{H_{\star}} \equiv (1-r)^2 \left(\frac{3\beta}{r} \right)^{3/2}. \quad (4.3)$$

Moreover, since H_{MD} is by definition the Hubble parameter such that the first term is the only term one must keep from expansion (4.1), we define,

$$\left(\frac{a_{\star}}{a} \right)_{\text{MD}} \equiv \frac{1}{(1-r)^{1/3}} \left(\frac{H_{\text{MD}}}{H_{\star}} \right)^{2/3} = 3\beta \frac{(1-r)}{r}. \quad (4.4)$$

We define the fraction of energy in Φ at the point matter domination ensues as

$$f_{\Phi, \text{MD}} \equiv \frac{1}{\frac{r}{(1-r)} \left(\frac{a_{\star}}{a} \right)_{\text{MD}} + 1} = \frac{1}{3\beta + 1}. \quad (4.5)$$

For $\beta = 1/3$ the second term in expansion (4.1) is $1/3$ the magnitude of the first, then matter domination ensues when the Φ matter accounts for half of the energy density of the universe: $f_{\Phi, \text{MD}} = 1/2$, just as matter domination was defined in [39].

Then the constraint that freeze-out occurs during matter domination may be expressed as,

$$T_F \lesssim T_{\text{MD}} \equiv T_{\star} \left(\frac{a_{\star}}{a} \right)_{\text{MD}} = 3\beta \frac{(1-r)}{r} T_{\star}, \quad (4.6)$$

which may also be written as,

$$T_{\star} \gtrsim \frac{1}{3\beta} \frac{r}{(1-r)} \frac{m_X}{x_F}. \quad (4.7)$$

It should be emphasized that what we mean by the Hubble parameter being “sufficiently small” is intimately linked to the r parameter. As we showed in expansion (3.47) when r is small, the terms up to linear order in r give approximately the first term of

expansion (3.46). We will derive below an $r_{\star, \text{MD}}$ which will represent the upper bound on r such that matter domination ensues immediately when $\Gamma = H_{\star}$, to demonstrate that it is not necessary for $\Gamma \ll H_{\star}$ in order to be in a matter domination scenario.

4.2 Freeze-out of dark matter before decay of Φ matter

Relative to the temperature T_{\star} (at which the energy density of Φ begins to evolve as a matter-like contribution) the temperature of the thermal bath which corresponds to the Φ lifetime is given by

$$T_{\Gamma} = T_{\star} \left(\frac{a_{\star}}{a} \right)_{\Gamma} \simeq \frac{T_{\star}}{(1-r)^{1/3}} \left(\frac{\Gamma}{H_{\star}} \right)^{2/3}, \quad (4.8)$$

Since, in this work we study the effects of entropy injections on a frozen-out population of dark matter, we require that dark matter freezes-out prior to Φ matter decay. This condition can be expressed as $T_F \gtrsim T_{\Gamma}$ and this can be written in terms of the reheat temperature using eq. (3.50)

$$T_F \equiv \frac{m_X}{x_F} \gtrsim \frac{T_{\text{RH}}^{4/3}}{[(1-r)\hat{\gamma}T_{\star}]^{1/3}} \quad (4.9)$$

Additionally, we should require that Φ dominates the energy density at the time of decay and thus $\rho_X \ll \rho_{\Phi}$. Indeed, this has been implicitly assumed in Section (2.2) when neglected the dark matter contribute to the interpolating Friedmann equation and we check this assumption now. This can be shown by comparing the dark matter freeze-out abundance to the Φ matter energy density at the point of freeze-out. For the sake of simplicity, we use the freeze-out abundance, $Y_{\infty} = Y_{\infty}^{\text{MD}}$, the freeze-out abundance that would occur in the limit that $r \rightarrow 0$. Since we will be mainly concerned in the $\Gamma \ll H_{\star}$ or small r regime, and we are only looking for an order of magnitude estimate, this should not affect the accuracy of this derivation (in fact, we arrive at generally more stringent

constraints than needed since the MD abundances before dilution are greater than those of RD). Notice that after freeze-out is complete,

$$\rho_X = m_X Y_\infty^{\text{MD}} s = m_X \left(3 \sqrt{\frac{5}{\pi}} \frac{\sqrt{g_*(T_*)} (n + 3/2) x_F^{n+3/2}}{g_{*S}(T_F) M_{\text{pl}} m_X \sigma_0 \sqrt{x_*}} \right) \left(\frac{2\pi^2}{45} g_{*S}(T_F) T^3 \right). \quad (4.10)$$

Furthermore,

$$T^3 = T_*^3 \left(\frac{a_*}{a} \right)^3 = T_*^3 \frac{\rho_\Phi}{(1-r)\rho_*}. \quad (4.11)$$

Plugging eq. (4.11) into eq. (4.10), taking $n = 0$, and parameterizing the cross section as $\sigma_0 = \alpha^2/m_X^2$, we have,

$$\frac{\rho_X}{\rho_\Phi} = \left[6 \sqrt{\frac{5}{\pi}} \frac{\sqrt{x_*} x_F^{3/2}}{(1-r) \sqrt{g_*(T_*)} \alpha^2} \right] \left(\frac{m_X}{M_{\text{Pl}}} \right). \quad (4.12)$$

Thus this fraction is parametrically of order

$$\frac{\rho_X}{\rho_\Phi} \sim 3 \times 10^{-13} \times \left(\frac{10^6 \text{ GeV}}{T_*} \right)^{1/2} \left(\frac{10^{-2}}{\alpha} \right)^2 \left(\frac{m_X}{1 \text{ TeV}} \right)^{3/2}. \quad (4.13)$$

Thus unless the annihilation rate of the dark matter is small (in which case it will likely freeze-out whilst relativistic) or the mass is very high then $\rho_X/\rho_\Phi \ll 1$. Thus assuming that the dark matter undergoes a period of freeze-out it is typically safe to assume that $\rho_{\text{DM}} \ll \rho_\Phi$ for $T < m_{\text{DM}}$. This implies that provided $\rho_\Phi > \rho_R$ then Φ dominates the energy density when it decays and, moreover, radiation domination is restored after Φ decay, as necessary for successful BBN. We discuss the requirements for reproducing the successes of BBN further in the next section.

4.3 Constraints on the reheating temperature

Big Bang Nucleosynthesis (BBN) is a remarkably successful theory in predicting the current cosmic abundances of light elements [5, 53]. Thus, any theory of DM should

respect its constraints as a benchmark for success [53]. The BBN period begins when the temperature of the bath $T \gg 1$ MeV, and at this temperature scale the proton to neutron ratio is roughly unity [5]. As the temperature drops to $T \simeq 1$ MeV the ratio of protons to neutrons changes beginning a series of events that eventually lead to the light element abundances we observe today [5]. So long as DM decoupling and entropy injections happen well before BBN onset, they will not interfere with BBN [53].

We thus require that DM be decoupled before the beginning of BBN and that the minimum temperature at its inception be $T_{\text{BBN}} \simeq 10$ MeV. Thus, the reheat temperature should be at least $T_{\text{RH}} \gtrsim T_{\text{BBN}}$, setting up the initial conditions for BBN. However, the reheat temperature is intrinsically tied to the relic density of dark matter in this scenario because of the dilution due to the entropy injection. Specifically the relic density of dark matter scales with dilution factor ζ as follows

$$(\Omega_X^{\text{MD}})^{\text{relic}} h^2 \sim 0.1 \cdot \left(\frac{m_X}{10^6 \text{ GeV}} \right)^{5/2} \left(\frac{0.1}{\alpha} \right)^2 \left(\frac{10^7 \text{ GeV}}{T_\star} \right)^{1/2} \left(\frac{\zeta}{10^{-4}} \right). \quad (4.14)$$

Since ζ is related to T_{RH} via eq. (3.55): $\zeta \approx \frac{g_\star(T_{\text{RH}})/g_\star(T_\star)}{(1-r)} \frac{T_{\text{RH}}}{T_\star}$, it follows that

$$T_{\text{RH}} \sim 10^3 \text{ GeV} \cdot \left(\frac{10^6 \text{ GeV}}{m_X} \right)^{5/2} \left(\frac{\alpha}{0.1} \right)^2 \left(\frac{T_\star}{10^7 \text{ GeV}} \right)^{3/2} \gtrsim T_{\text{BBN}}. \quad (4.15)$$

Thus the requirement of reproducing BBN observables bounds the parameter space, we will give an example shortly which demonstrates how these bounds manifest.

Furthermore, if the dark matter is produced via Φ decays, then it can have two components, an initial thermal component which freezes-out during matter domination and a component associated with the direct decay products of Φ . To restrict to the case of matter dominated freeze-out we assume that Φ does not decay non-thermally to dark matter. However, since the dark matter couples to the thermal bath, if the Φ decay implies a reheat temperature comparable to the freeze-out temperature, then

interactions in the bath can lead to dark matter production. Thus to focus on the clean regime of freeze-out during matter domination followed by dilution we require $T_{\text{RH}} \ll T_F$. Comparing eqs. (3.10) & (4.15) both T_{RH} and T_F are controlled by m_X , α and T_\star thus this constraint also significantly constrains the parameter space, as we illustrate shortly. We will discuss in more detail the case of $T_{\text{RH}} \sim T_F$, which is a consistent and interesting alternate scenario for dark matter freeze-out, in the next Chapter.

4.4 Ordering of scales

As discussed in Section 2.3 the matter dominated freeze-out scenario relies on an assumed ordering of scales

$$T_\star \geq T_{\text{MD}} \gg T_F \gg T_\Gamma \quad (4.16)$$

This implies that a period of matter domination occurs, then subsequent dark matter freezes out and after which the matter-like state Φ decays. Thus in this section we briefly comment on the implications this ordering applies on the relative size of different parameters.

Specifically, here we address the requirements

- 4a. Decay of Φ matter occurs below T_\star and T_{MD} .
- 4b. Freeze-out temperature of dark matter is less than T_\star and T_{MD} .
- 4c. The reheat temperature does not exceed T_\star and T_{MD} .

Note that the lifetime of Φ is controlled by an independent coupling and thus T_Γ (the temperature T of the bath at $H \sim \Gamma$) can be set independently of the other parameters in the model.

If Φ matter decays prior to matter domination, not only will the entropy injection be small, but freeze-out would not occur prior to decay when satisfying the constraint of Section 4.1. Therefore we require that,

$$\Gamma \lesssim H_{\text{MD}} \equiv (1-r)^2 \left(\frac{3\beta}{r}\right)^{3/2} H_{\star}, \quad (4.17)$$

which by using approximation (3.56) may be written as,

$$T_{\text{RH}} \lesssim \hat{\gamma}^{1/4} (1-r) \left(\frac{3\beta}{r}\right)^{3/4} T_{\star}. \quad (4.18)$$

It is required that the decay of Φ matter when the bath is at temperature T_{Γ} occurs below T_{\star} , the relative orderings of these scales can be checked by inspection of the Friedmann equation. In the Friedmann equation (2.18) there is an implicit Θ -function, such that above temperature T_{\star} all energy is radiation, and below which the matter component appears. Moreover, matter domination may ensue immediately at T_{\star} . For example, for $H_{\text{MD}} = H_{\star}$ this would imply

$$r_{\star, \text{MD}} \equiv r|_{H_{\text{MD}}=H_{\star}} = \frac{1}{(3\beta)^{-1} + 1} \quad (4.19)$$

with $\beta = 1/3$, this corresponds to a value $r = 0.5$. Thus, if matter constitutes greater than 50% of energy at T_{\star} , matter domination begins immediately at T_{\star} . Requiring that Φ decay does not occur above T_{\star} implies the constraint $\Gamma \lesssim H_{\star}$, or in terms of temperatures

$$T_{\text{RH}} \lesssim \hat{\gamma}^{1/4} T_{\star}. \quad (4.20)$$

Furthermore, since our analysis of the Friedman equations fixes an initial condition at $T = T_{\star}$ it follows that for our analysis to be valid all temperature scales which we are interested should be below or equal to T_{\star} , including the freeze-out temperature of dark matter: $m_X/x_F = T_F \lesssim T_{\star}$.

4.5 Summary

Above we have explored the various constraints, before closing this section we summarize the leading constraints and show how they apply for a particular example. We assume the ordering of scales $T_\star \gg T_{\text{RH}}, T_F, T_\Gamma$, as discussed above.

As discussed in Section 4.1 the dark matter should decouple only after the universe is matter dominated: $T_{\text{MD}} \gtrsim T_F^{\text{RD}}$ (excluded region shaded red in Fig. 4.1). Thus we should compare the radiation dominated freeze-out temperature to T_{MD} derived in eq. (4.6). This also implies that Φ decays only after it comes to dominate the energy density of the universe. From eq. (3.48) & (4.6) one can verify that $T_{\text{MD}} \gg T_\Gamma$ provided that $T_\star \gg T_{\text{RH}}$. Furthermore, as in Section 4.2, the dark matter should decouple prior to the period of Φ decays: $T_\Gamma \lesssim T_F^{\text{MD}}$ (purple in Fig. 4.1).

In Section 4.3 we argued that to avoid conflict with BBN we require $T_{\text{RH}} \gtrsim 10$ MeV (grey in Fig. 4.1). Both T_{RH} and the dark matter relic density are controlled by ζ and T_\star , but these requirements can generally be simultaneously satisfied. Higher reheat temperatures are often desirable for baryogenesis mechanisms, e.g. electroweak baryogenesis [54] typically requires $T_{\text{RH}} \gtrsim 100$ GeV (blue in Fig. 4.1). Moreover, to remain in the matter dominated freeze-out regime we require $T_F \gg T_{\text{RH}}$ (green in Fig. 4.1). The yellow region indicates where we expect the instantaneous decay approximation to be unreliable, which we discuss more in the next Chapter. Additionally, to restore radiation domination after Φ decays, it is necessary that the the dark matter energy density remains small relative to that of Φ immediately prior to Φ decays. Since the the dark matter number density is Boltzmann suppressed, $\rho_\Phi \gg \rho_X$ at $T = T_F$ and this requirement is typically readily satisfied.

Finally, the observed the dark matter relic density must be reproduced ($\Omega_{\text{DM}} h^2 \sim 0.1$), as determined by eq. (3.40). In Figure 4.1 we show how the parameter space is constrained by the requirements above for s -wave annihilations with $\alpha = 0.1$, where we take $T_\star \simeq m_\Phi$ (thus $r \approx 0.99$), and we neglect changes in g_\star .

Observe that the leading constraints are due to the requirement that the dark matter decouples after the universe is Φ matter dominated (shaded red) and $T_F \gg T_{RH}$ (green/yellow). Requiring a reheat temperature above the electroweak phase transition $T_{RH} \gtrsim 100$ GeV (blue) further constrains the parameter space. For the parameter choices made in Figure 4.1, the model prefers heavier dark matter, and can accommodate TeV scale dark matter.

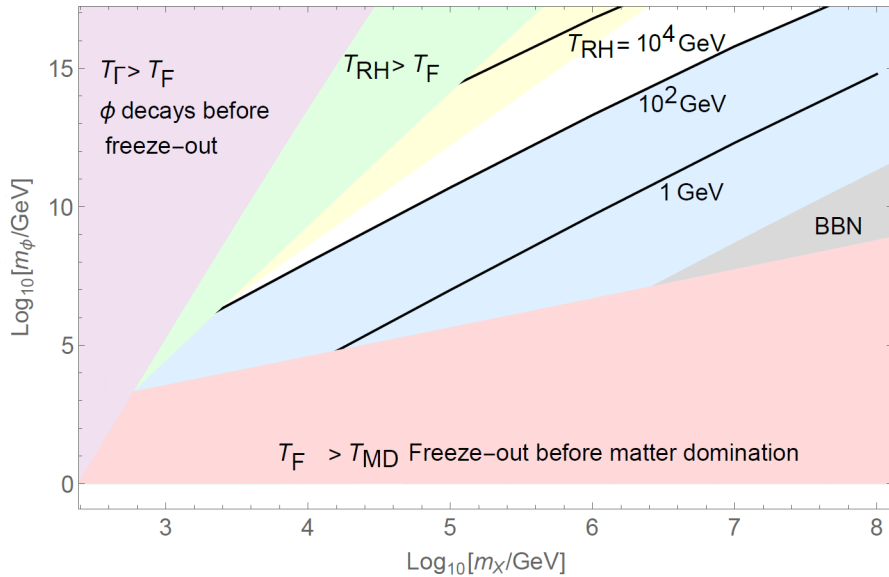


Figure 4.1: Parameter space of matter dominated DM freeze-out assuming an s -wave annihilation with $\sigma_0 \equiv \alpha^2/m_X^2$ for $\alpha = 0.1$ with $T_\star \simeq m_\Phi$, and $r \approx 0.99$. We show contours of T_{RH} which reproduce the dark matter relic density. The main constraints are that the dark matter decouples prior to Φ decays (purple), but after the universe is Φ matter dominated (red). We also require $T_F > T_{RH}$ (green), in the yellow region the instantaneous decay approximation is less reliable. We shade regions in which the reheat temperature is low: for $T_{RH} \lesssim 10$ MeV BBN observables are disrupted (grey) and for $T_{RH} \lesssim 100$ GeV baryogenesis is challenging (blue).

Chapter 5

Beyond Instantaneous Decay

This chapter presents original results which have not been previously presented.

In the previous chapter we assumed an instantaneous decay and thermalization at $t \sim \Gamma^{-1}$. In this chapter we take a closer look at the equations governing the decay of a massive species or oscillating scalar field. We also derive constraints that assure accuracy in assuming instantaneous decay in the previous chapter.

5.1 Decay Equations

The equation governing the decay of a coherently oscillating field or massive particle species Φ is as follows

$$\dot{\rho}_\Phi + 3H\rho_\Phi = -\Gamma\rho_\Phi, \quad (5.1)$$

which may be written in a more suggestive form as

$$\frac{d}{dt}(\rho_\Phi a^3) = -\Gamma(\rho_\Phi a^3). \quad (5.2)$$

Integrating from time t_* , the time when coherent oscillations of a scalar field begin or a decaying particle species begins to evolve as matter¹, to time t we have

$$\rho_\Phi = \rho_{\Phi_*} \left(\frac{a_*}{a}\right)^3 e^{-\tau}, \quad (5.3)$$

¹This time will roughly be $t_* \sim H_*^{-1}$ but here we keep the analysis general.

where $\rho_{\Phi\star}$ is the energy density of the Φ matter at t_\star , and $\tau \equiv \Gamma t$. Expanding (5.3) in powers of τ

$$\rho_\Phi = \rho_{\Phi\star} \left(\frac{a_\star}{a}\right)^3 (1 + \mathcal{O}(\tau^1)). \quad (5.4)$$

From relation (2.9) we also have $a(t) \propto t^{\frac{2}{3}(1+w)^{-1}}$ (recall that $w = 0$ for MD and $w = 1/3$ for RD), hence

$$\frac{a_\star}{a} = \left(\frac{t_\star}{t}\right)^{\frac{2}{3}(1+w)^{-1}}. \quad (5.5)$$

Thus, collecting only the $\mathcal{O}(\tau^0)$ term of expansion (5.4) and using eq. (5.5) we have

$$\rho_\Phi \approx \rho_{\Phi\star} \left(\frac{t_\star}{t}\right)^{2(1+w)^{-1}}. \quad (5.6)$$

Assuming that Φ matter decays solely to the radiation sector, the equation governing the radiation energy density is

$$\dot{\rho}_r + 4H\rho_r = \Gamma\rho_\Phi, \quad (5.7)$$

which may be rewritten as

$$\frac{d}{dt}(\rho_r a^4) = \Gamma\rho_\Phi a^4. \quad (5.8)$$

Using approximation (5.6) and relation (5.5), eq. (5.8) may be approximated as

$$\frac{d}{dt}(\rho_r a^4) \simeq \Gamma\rho_{\Phi\star} \left(\frac{t_\star}{t}\right)^{2(1+w)^{-1}} a^4 \simeq \Gamma\rho_{\Phi\star} a_\star^4 \left(\frac{t_\star}{t}\right)^{-(2/3)(1+w)^{-1}} \quad (5.9)$$

Integrating equation (5.9) from t_\star to t gives

$$\rho_r \simeq \rho_{r\star} \left(\frac{a_\star}{a}\right)^4 + \rho_{\Phi\star} \left(\frac{a_\star}{a}\right)^4 \frac{1}{(2/3)(1+w)^{-1} + 1} \left(\tau \left(\frac{\tau_\star}{\tau}\right)^{-(2/3)(1+w)^{-1}} - \tau_\star \right), \quad (5.10)$$

where $\tau_\star = \Gamma t_\star$. In [40] they refer to the first term on the RHS of equation (5.10) as the ‘‘old’’ radiation and the latter term as the ‘‘new’’ radiation. We will adopt the same

naming conventions here. Writing equation (5.10) solely in terms of τ gives

$$\rho_r \simeq \rho_{r\star} \left(\frac{\tau_\star}{\tau}\right)^{(8/3)(1+w)^{-1}} + \frac{\rho_{\Phi\star}}{(2/3)(1+w)^{-1} + 1} \left(\tau \left(\frac{\tau_\star}{\tau}\right)^{2(1+w)^{-1}} - \tau_\star \left(\frac{\tau_\star}{\tau}\right)^{(8/3)(1+w)^{-1}} \right). \quad (5.11)$$

Notice that when $\tau_\star \ll 1$ the last term on the RHS of equation (5.11) may be neglected (as they have done in [40]), but here we keep it for completeness. Defining

$$\mathcal{T} \equiv \tau_\star/\tau = t_\star/t \quad (5.12)$$

and using $\rho_{r\star} = r\rho_\star$ and $\rho_{\Phi\star} = (1-r)\rho_\star$, we write eq. (5.11) as

$$\frac{\rho_r}{\rho_\star} \simeq r\mathcal{T}^{(8/3)(1+w)^{-1}} + \frac{(1-r)\tau_\star}{(2/3)(1+w)^{-1} + 1} \left(\mathcal{T}^{2(1+w)^{-1}-1} - \mathcal{T}^{(8/3)(1+w)^{-1}} \right). \quad (5.13)$$

5.2 Breakdown of Entropy Conservation in the Bath

In [40] they find that the entropy remains roughly constant until the first and second terms (or old and new radiation terms, respectively) on the RHS of equation (5.13) become comparable. We call this point at which the assumption of entropy conservation is violated \mathcal{T}_{EV} and thus define \mathcal{T}_{EV} implicitly by

$$r\mathcal{T}_{\text{EV}}^{(8/3)(1+w)^{-1}} \equiv \frac{(1-r)\tau_\star}{(2/3)(1+w)^{-1} + 1} \left(\mathcal{T}_{\text{EV}}^{2(1+w)^{-1}-1} - \mathcal{T}_{\text{EV}}^{(8/3)(1+w)^{-1}} \right). \quad (5.14)$$

Solving (5.14) for \mathcal{T}_{EV} , and letting $v \equiv (2/3)(1+w)^{-1} + 1$ for concision, we have

$$\mathcal{T}_{\text{EV}} = \left(1 + \left(\frac{r}{1-r} \right) \frac{v}{\tau_\star} \right)^{-1/v} \quad (5.15)$$

Our freeze-out and abundance calculations in Chapter 3, and constraints in Chapter 4 relied on the assumption of constant entropy until an instantaneous decay occurs at $t \sim \Gamma^{-1}$. Instead considering an exponential decay law (as in [40]), there is still a considerable

parameter space to allow freeze out to occur prior to non-negligible contributions of entropy. The precise time when this occurs is given by eq. (5.15).

We fixed $T_\star = 10^7$ GeV, $r = 0.99$, $T_{\text{RH}} = 10$ MeV, and w is taken to be an affine interpolation between RD ($w = 1/3$) and MD ($w = 0$) values and plot the evolution of the system in the top panel of Figure 5.1. The w interpolation is weighted linearly according to the relative fraction of energy that radiation and matter constitute, and is plotted as the dashed line in Figure 5.1. The vertical black line shows the point at which $T = T_{\text{EV}}$. Notice that despite the Φ matter (whose fraction of the total energy is the blue line, and radiation's fraction is the red line) constituting only 1% of the energy of the universe at τ_\star , it comes to dominate relatively early on during decays, and only precipitously falls near $\tau = 1$ (or $t \sim \Gamma^{-1}$).

Figure 5.1 also shows that it is possible to have a large amount of time between when MD ensues (when matter constitutes half the energy, hence when the red and blue line intersect) till when entropy violations become considerable. The new aspect of dark matter which this thesis (and the associated paper [1]) presents is the possibility of freeze-out in the matter dominated regime which had been previously unstudied. This difference between our work and previous related scenarios (such as [6]) is most clearly illustrated in the lower panel of Figure 5.1 which shows that the time of freeze-out (black curve) can readily fall between when matter domination begins (red shaded region is radiation dominated) and when entropy violations are large (yellow shaded region). For the bottom of Figure 5.1 T_{RH} was not fixed as in the top (the rest of the parameters were fixed the same); instead (3.55) was used to ensure that the observed DM relic density was matched.

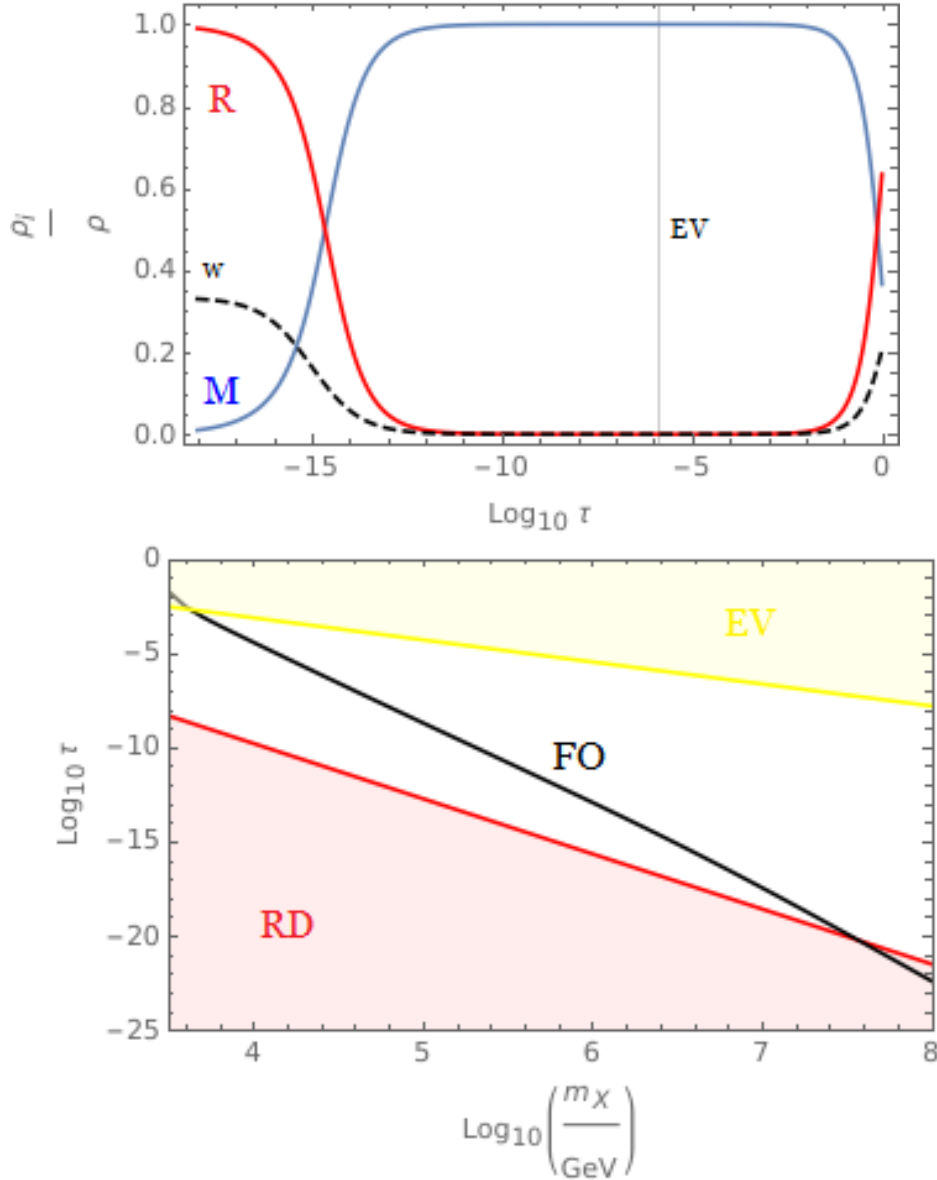


Figure 5.1: Logarithmic time scales and orderings of relevant events for MD freeze-out scenario from $\tau = \tau_*$ till $\tau = 1$ ($t \sim \Gamma^{-1}$) for $T_* = 10^7$ GeV and $r = 0.99$. Top: fraction of energy density in matter (blue) and radiation (red), for $T_{\text{RH}} = 10$ MeV and w (dashed) parameterized between RD ($w = 1/3$) and MD ($w = 0$). Vertical line represents moment when entropy violation is considerable, and first intersection of blue and red line signifies MD onset. Bottom: logarithmic time of freeze-out versus DM mass (black) for T_{RH} required to produce observed DM relic density. RD era shaded in red and times of considerable entropic violations shaded in yellow; adiabatic MD freeze-out occurs between shaded regions.

Let $t_{\text{EV}} \equiv t_\star/\mathcal{T}_{\text{EV}}$, which from relation (5.5) corresponds to scale factor

$$(a_\star/a)_{\text{EV}} \equiv (t_\star/t_{\text{EV}})^{v-1} \quad (5.16)$$

Then, because entropy remains roughly constant until $a = a_{\text{EV}}$, we may use the $T \propto a^{-1}$ relation during the period while entropy remains constant to obtain the temperature which corresponds to $T(a_{\text{EV}})$. Notably, $T \propto a^{-1}$ is not valid once the approximation of entropy conservation is strongly perturbed. To obtain an expression for T_{EV} we consider the evolution from $T = T_\star$

$$T_{\text{EV}} \equiv T_\star(a_\star/a)_{\text{EV}} \simeq T_\star(t_\star/t_{\text{EV}})^{v-1} \quad (5.17)$$

Using the definition $\mathcal{T}_{\text{EV}} \equiv (t_\star/t_{\text{EV}})$ it follows

$$T_{\text{EV}} \simeq T_\star \mathcal{T}_{\text{EV}}^{v-1} \simeq T_\star \left(1 + \left(\frac{r}{1-r} \right) \frac{v}{\tau_\star} \right)^{(1-v)/v}. \quad (5.18)$$

Therefore the requirement of constant entropy during freeze-out implies an additional constraint in the event of non-instantaneous decay:

$$T_F \gtrsim T_{\text{EV}}. \quad (5.19)$$

For a more precise derivation of the temperature of the thermal bath at any given moment we should track changes in the degrees of freedom, we may use equation (5.13) since

$$\frac{T}{T_\star} = \left(\frac{g_\star(T_\star) \rho_r}{g_\star(T) \rho_\star} \right)^{1/4} \quad (5.20)$$

Then, by eq. (5.15) in (5.13) we find that T_{EV} may also be defined as

$$T_{\text{EV}} \equiv T_\star \left(\frac{g_\star(T_\star) \rho_r}{g_\star(T) \rho_\star} \right)^{1/4} \Big|_{\mathcal{T}=\mathcal{T}_{\text{EV}}}. \quad (5.21)$$

Writing out (5.21) explicitly, with the aid of eq. (5.13) and eq. (5.15)

$$T_{\text{EV}} \simeq T_{\star} \left(\frac{g_{\star}(T_{\star})}{g_{\star}(T_{\text{EV}})} \right)^{1/4} \left[r \mathcal{T}_{\text{EV}}^{4(v-1)} + \frac{(1-r)\tau_{\star}}{v} \left(\mathcal{T}_{\text{EV}}^{3v-4} - \mathcal{T}_{\text{EV}}^{4(v-1)} \right) \right]^{1/4}. \quad (5.22)$$

But by definition of \mathcal{T}_{EV} , the two terms in the square bracket must be equal, so that the value within the square bracket is $2r\mathcal{T}_{\text{EV}}^{4(v-1)}$, and thus T_{EV} may be written as

$$T_{\text{EV}} \simeq T_{\star} (2r)^{1/4} \left(\frac{g_{\star}(T_{\star})}{g_{\star}(T_{\text{EV}})} \right)^{1/4} \left(1 + \left(\frac{r}{1-r} \right) \frac{v}{\tau_{\star}} \right)^{(1-v)/v} \quad (5.23)$$

Unless there are significant numbers of new states at high temperatures we expect $g_{\star}(T_{\star})/g_{\star}(T_{\text{EV}}) \sim \mathcal{O}(1)$ and thus this gives a similar result to eq. (5.18) above.

5.3 Hubble Parameter During Decays

When entropy produced by Φ decays becomes comparable to the entropy due to the old radiation the assumption of constant entropy per comoving volume ceases to hold. Moreover, even if freeze-out occurred during the time prior to significant entropy injection, the changing dynamics of the universe can conceivably cause a frozen-out species to recouple solely due to the changing relationship between the Hubble parameter and temperature, thus altering the freeze-out temperature. This is because the Hubble parameter in the RD and MD case have relation $H_{\text{RD}} \propto T^2$ and $H_{\text{MD}} \propto T^{3/2}$, but if entropy injection becomes significant $H_{\text{EV}} \propto T^4$.

Freeze-out temperature is defined by the condition $H = \Gamma_{\text{ann}}$, thus a change in the relationship between the Hubble parameter and temperature changes the freeze-out temperature also. Below we derive a general freeze-out temperature that encompasses various scenarios and derive a constraint to ensure that dark matter is not repopulated.

First we derive a relation between temperature and scale factor during decays, fol-

lowing [6]. From eq. (5.5), and defining $\mathcal{A} \equiv a_*/a$, we have that,

$$\mathcal{T} = \mathcal{A}^{1/(v-1)} = \mathcal{A}^{(3/2)(1+w)}. \quad (5.24)$$

The decay equations prior to $t \sim \Gamma^{-1}$ may also be written in terms of \mathcal{A} thusly

$$\frac{\rho_r}{\rho_*} \simeq r\mathcal{A}^4 + \frac{(1-r)\tau_*}{v} (\mathcal{A}^{4\bar{v}} - \mathcal{A}^4), \quad \frac{\rho_\Phi}{\rho_*} \simeq (1-r)\mathcal{A}^3, \quad (5.25)$$

where $\bar{v} \equiv ((3/4)v-1)/(v-1)$. Since $\bar{v} < 1$ (strictly this is true only for $v > 0$, which is our concern), the term in (5.25) proportional to $\mathcal{A}^{4\bar{v}}$ will eventually come to dominate prior to $t \sim \Gamma^{-1}$ when r is sufficiently small; the precise conditions were derived above with \mathcal{T}_{EV} . For the temperature versus scale factor relation, we use (5.20) and (5.25) to obtain

$$T \simeq T_* \left(\frac{g_*(T_*)}{g_*(T)} \right)^{1/4} \left[r\mathcal{A}^4 + \frac{(1-r)\tau_*}{v} (\mathcal{A}^{4\bar{v}} - \mathcal{A}^4) \right]^{1/4} \quad (5.26)$$

If the $\mathcal{A}^{4\bar{v}}$ comes to dominate, and $\bar{v} = 3/8$, then we have the relation $T \propto a^{-3/8}$ found in [6] and [40]. Furthermore, the Hubble parameter during decay is given by

$$H \simeq H_* \left[\frac{\rho_r}{\rho_*} + \frac{\rho_\Phi}{\rho_*} \right]^{1/2} \simeq H_* \left[r\mathcal{A}^4 + \frac{(1-r)\tau_*}{v} (\mathcal{A}^{4\bar{v}} - \mathcal{A}^4) + (1-r)\mathcal{A}^3 \right]^{1/2} \quad (5.27)$$

The requirement that DM is not repopulated during decays can be expressed using the results above. For MD freeze-out, we require that $H(T_F) = \Gamma_{\text{ann}}$ occur while $T \propto a^{-1}$ and the matter component dominates the energy density. This is achieved with $T_F \gtrsim T_{\text{EV}}$, as derived above. A more general freeze-out temperature may be obtained by using eq. (5.27) as a function of temperature (by inverting eq. (5.26)), and setting this equal to the annihilation rate. Requiring DM is frozen out (i.e. $H(T) \gtrsim \Gamma_{\text{ann}}(T)$) before decays are important implies $\tau_* \lesssim \mathcal{T}(T_F) \lesssim \mathcal{T}_{\text{EV}}$ or equivalently

$$T_* \lesssim T_F \lesssim T_{\text{EV}} \quad (5.28)$$

Let us now make the following assumptions that will make the above analysis simpler. First, assume that $t_\star = H_\star^{-1}$, implying

$$\tau_\star = \frac{\Gamma}{H_\star} \approx \hat{\gamma}^{-1/2} \left(\frac{T_{\text{RH}}}{T_\star} \right)^2, \quad (5.29)$$

where the approximation comes from (3.56). Second, assume $\tau_\star \ll 1$. Third, assume that r is sufficiently small such that immediately at T_\star matter domination ensues. This can be achieved by taking $r \lesssim 0.5$ when $\beta = 1/3$. This will allow us to take $w = 0$, or equivalently $v = 5/3$ or $\bar{v} = 3/8$, from time $t = H_\star^{-1}$ till time $t = \Gamma^{-1}$. This simplifies our analysis since there is no time in the domain we are interested in where radiation is dominant². Our fourth assumption will be that temperature is always falling, and never rises. From (5.31), which is derived in the next section, this requirement can be expressed as $\tau_\star < 8r/3(1-r)$.

With these simplifying assumptions we can approximate T_{EV} as follows

$$T_{\text{EV}} \approx T_\star \left(\frac{3}{5} \right)^{2/5} \left(\frac{1-r}{r} \right)^{2/5} \hat{\gamma}^{1/5} \left(\frac{T_{\text{RH}}}{T_\star} \right)^{4/5}. \quad (5.30)$$

For $T \gtrsim T_{\text{EV}}$ we assume $T \propto a^{-1}$, and for $T \lesssim T_{\text{EV}}$ then $T \propto a^{-3/8}$. We also assume that the energy density continues to be dominated by matter until $t = \Gamma^{-1}$. Thus to evaluate the requirement that $T_F > T_{\text{EV}}$ one can compare eq. (5.30) to eq. (3.10)

Returning to Figure 4.1, here we illustrated the parameter space for a characteristic model and the yellow shaded region shown here indicates the region in which entropy conservation is no longer a good approximation. Specifically, the yellow shading indicates the parameter region in which $T_F < T_{\text{EV}}$, and thus the dynamics of freeze-out are no longer matter dominated freeze-out but rather decoupling during a period of entropy injection as described above. This latter scenario is reminiscent to that studied in [6].

²This assumption is not necessary, if an interpolation of w is used and with matter constituting only 1% of the energy density at τ_\star , MD ensues much earlier than entropy violation as shown in Figure 5.1

5.4 Temperature Maxima During Decay

Although the decay of a massive species or coherent oscillations of a scalar field are said to “reheat” the universe, the temperature need not rise during this reheating [40]. In [6] it is shown that after an initial rise in temperature to what is termed T_{MAX} , the temperature actually *falls* to T_{RH} . This is why, in [6], Giudice, Kolb and Riotto define T_{RH} as the highest temperature of the radiation domination era. Thus after the temperature of the bath falls below T_{RH} , radiation comprises the dominant component of the universe’s energy. In [6] they consider decay in the absence of “old” radiation (i.e. $\rho_{r\star} \approx 0$). We next comment on the case omitted in [6], which includes an old radiation component and we derive a more general T_{MAX} than [6].

To find the time at which the temperature is at an extremum, we find the critical point of eq. (5.13) with respect of \mathcal{T} , which gives

$$\mathcal{T}_{\text{MAX}} = \bar{v}^{1/v} \left(1 - \left(\frac{r}{1-r} \right) \frac{v}{\tau_\star} \right)^{-1/v} \quad (5.31)$$

Thus for a sensible analysis, we require $\tau_\star < \mathcal{T}_{\text{MAX}} < 1$ (otherwise the time that the maximum temperature occurs after $t \sim \Gamma^{-1}$ or prior to t_\star). For the τ_\star lower bound and $v > 0$, these give $\tau_\star^v - (r/(1-r))v\tau_\star^{v-1} < \bar{v}$. The $\mathcal{T}_{\text{MAX}} < 1$ upper bound gives $\tau_\star > 4(v-1)r/(1-r)$. Whenever any of these bounds are violated, which is readily achievable as shown in the previous section, there will be no physical extremum of temperature. Thus the temperature smoothly continues dropping as the universe expands, and the global maximum of temperature would be T_\star . To obtain the temperature when a local maximum is present, we insert (5.31) into (5.20) and (5.13) to obtain

$$T_{\text{MAX}} \simeq T_\star \left(\frac{g_*(T_\star)}{g_*(T_{\text{MAX}})} \right)^{1/4} \left[r\mathcal{T}_{\text{MAX}}^{4(v-1)} + \frac{(1-r)\tau_\star}{v} \left(\mathcal{T}_{\text{MAX}}^{3v-4} - \mathcal{T}_{\text{MAX}}^{4(v-1)} \right) \right]^{1/4} \quad (5.32)$$

This generalizes the result of [6] to include an “old” radiation component and, furthermore, for $r = 0$ we recover the result of [6].

Chapter 6

Matter Dominated Freeze-out via the Higgs Portal

This chapter presents original results which have not been previously presented.

In previous chapters we studied a model-independent, matter-dominated freeze-out scenario for dark matter. We found that there was a considerable amount of viable parameter space for a wide range of dark matter mass and annihilation cross-section values. Here we take our previous work on matter-dominated freeze-out and apply it to the specific model of dark matter annihilations through the Higgs Portal.

Very little is known about the interactions of dark matter, but possible interactions with the Higgs boson provide a promising means to link dark matter to the Standard Model [55–58]. The precise relations of the Higgs Portal depend on the nature of the dark matter quantum numbers, in this thesis we consider only the case of a real scalar dark matter particle φ , whose Lagrangian terms are \mathbb{Z}_2 invariant

$$\mathcal{L} = \mathcal{L}_{\text{SM}} + \frac{1}{2}\partial_\mu\varphi\partial^\mu\varphi - \frac{1}{2}\mu^2\varphi^2 - \frac{1}{4!}\lambda\varphi^4 - \frac{1}{2}\kappa\varphi^2 H^\dagger H \quad (6.1)$$

where H is the Standard Model Higgs and \mathcal{L}_{SM} is the Standard Model Lagrangian.

Thus this extension of \mathcal{L}_{SM} corresponds to one real scalar DM particle with a coupling κ to the Higgs boson. Although μ and λ are often reserved for the Higgs quadratic and quartic couplings, since we won't make reference to these quantities, we use these instead for the φ couplings; importantly they are unrelated to the Higgs coupling.

Once the Higgs boson acquires vacuum expectation value $\langle H \rangle = v_0$ after electroweak symmetry breaking [59–61], and using the Unitary Gauge so that $H^\dagger = (0, (v_0 + h)/\sqrt{2})$, the Lagrangian may be expanded around this value giving

$$\mathcal{L} = \mathcal{L}_{\text{SM}} + \frac{1}{2}\partial_\mu\varphi\partial^\mu\varphi - \frac{1}{2}\mu^2\varphi^2 - \frac{1}{4!}\lambda\varphi^4 - \frac{1}{4}\kappa\varphi^2h^2 - \frac{1}{4}\kappa\varphi^2v_0^2 - \frac{1}{2}\kappa\varphi^2v_0h. \quad (6.2)$$

Thus, the mass of the scalar DM particle is given by

$$m_\varphi^2 = \mu^2 + \frac{1}{2}\kappa v_0^2, \quad (6.3)$$

and the Higgs decay width to φ is

$$\Gamma(h \rightarrow \varphi\varphi) = \frac{\kappa^2 v_0^2}{32\pi m_h} \sqrt{1 - \frac{4m_\varphi^2}{m_h^2}}, \quad (6.4)$$

where m_h is the Higgs boson mass. Note that the unbroken \mathbb{Z}_2 symmetry which stabilises the dark matter also forbids φ from obtaining a non-zero vacuum expectation value.

6.1 Dark Matter Annihilation to Standard Model States

For the model-independent approach taken above, we parameterized the thermally-averaged cross-section of dark-matter annihilation to SM particles by parameterizing the cross section as $\sigma_0 = \alpha^2/m_X^2$. In this section we derive the Higgs Portal amplitudes for various DM annihilations to the SM particles, concluding with the total center-of-mass frame, thermally-averaged annihilation cross-section.

The three main annihilation routes for scalar DM via the Higgs portal are

- Dark matter to Standard Model Fermions, $\varphi\varphi \rightarrow f\bar{f}$,
- Dark matter to Standard Model Vector Bosons, $\varphi\varphi \rightarrow V\bar{V}$
- Dark matter to Higgs Bosons, $\varphi\varphi \rightarrow hh$

which we explore in order below.

Dark matter to Standard Model Fermions, $\varphi\varphi \rightarrow f\bar{f}$

Figure 6.1 shows the DM annihilation to two fermions, the amplitude for which is ,

$$i\mathcal{M}_{\varphi\varphi \rightarrow f\bar{f}} = (1)(-i\kappa v_0)(1)\frac{i}{q^2 - m_h^2 + im_h\Gamma_h}\bar{u}^r(p_f)\left(-i\frac{m_f}{v_0}\right)v^s(p_{\bar{f}}). \quad (6.5)$$

where m_f is the mass of the fermion and Γ_h is the total width of the Higgs boson. The cross-section for this process, in the center-of-mass (CM) frame is then

$$\sigma_{\varphi\varphi \rightarrow f\bar{f}} = \frac{1}{16\pi s} \frac{\sqrt{1 - 4m_f^2/s}}{\sqrt{1 - 4m_\varphi^2/s}} \sum_{\text{spin,color}} |\mathcal{M}_{\varphi\varphi \rightarrow f\bar{f}}|^2, \quad (6.6)$$

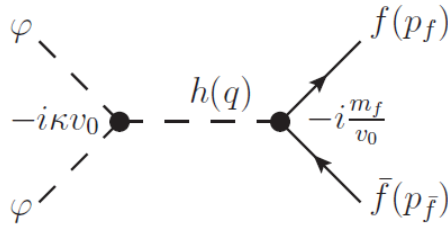


Figure 6.1: Dark Matter to Standard Model Fermions, $\varphi\varphi \rightarrow f\bar{f}$

where s is the Mandelstam variable. Carrying out the sum over spin and color gives

$$\begin{aligned}
\sum_{\text{color,spin}} |\mathcal{M}_{\varphi\varphi\rightarrow f\bar{f}}|^2 &= \frac{N_c \kappa^2 m_f^2}{(s - m_h^2)^2 + m_h^2 \Gamma_h^2} \sum_{r,s} \bar{u}^r(p_f) v^s(p_{\bar{f}}) (\bar{u}^r(p_f) v^s(p_{\bar{f}}))^* \\
&= \frac{N_c \kappa^2 m_f^2}{(s - m_h^2)^2 + m_h^2 \Gamma_h^2} \text{tr} \left[(\not{p}_f + m_f) (\not{p}_{\bar{f}} - m_f) \right] \\
&= \frac{N_c \kappa^2 m_f^2}{(s - m_h^2)^2 + m_h^2 \Gamma_h^2} (4p_f p_{\bar{f}} - 4m_f^2) = \frac{2N_c \kappa^2 m_f^2 (s - 4m_f^2)}{(s - m_h^2)^2 + m_h^2 \Gamma_h^2},
\end{aligned} \tag{6.7}$$

where N_c is the number of colors, which we take to be equal to 3 for quarks and 1 for leptons. The cross-section is then

$$\sigma_{\varphi\varphi\rightarrow f\bar{f}} = \frac{N_c \kappa^2 m_f^2}{8\pi s} \frac{\sqrt{1 - 4m_f^2/s}}{\sqrt{1 - 4m_\varphi^2/s}} \frac{s - 4m_f^2}{(s - m_h^2)^2 + m_h^2 \Gamma_h^2}. \tag{6.8}$$

Letting $r_i \equiv m_i/2m_\varphi$, $r_\Gamma \equiv m_h \Gamma_h/4m_\varphi^2$, and v be the relative velocity between the two incoming particles (in the CM frame, $v \approx 2v_1$ in the non-relativistic limit, where v_1 is the velocity of the incoming particles), we expand the cross-section multiplied by v in powers of relative velocity thusly

$$\sigma_{\varphi\varphi\rightarrow f\bar{f}} v = \sigma_{\varphi\varphi\rightarrow f\bar{f}}^{(0)} + \sigma_{\varphi\varphi\rightarrow f\bar{f}}^{(2)} v^2 + \mathcal{O}(v^4), \tag{6.9}$$

where

$$\sigma_{\varphi\varphi\rightarrow f\bar{f}}^{(0)} \equiv \frac{\kappa^2}{16\pi m_\varphi^2} \frac{r_f^2 (1 - 4r_f^2)^{3/2}}{(1 - r_h^2)^2 + r_\Gamma^2} \tag{6.10}$$

and

$$\sigma_{\varphi\varphi\rightarrow f\bar{f}}^{(2)} \equiv \frac{\kappa^2}{32\pi m_\varphi^2} \frac{r_f^2 (1 - 4r_f^2)^{1/2} (1 - 7r_f^2 + r_h^2 (1 - 10r_f^2) + 3r_f^2 (r_h^4 + r_\Gamma^2))}{((1 - r_h^2)^2 + r_\Gamma^2)^2}. \tag{6.11}$$

Dark matter to Standard Model Vector Bosons, $\varphi\varphi \rightarrow V\bar{V}$

The amplitude for the diagram in Figure 6.2, for the s-channel DM annihilation to two vector bosons, where m_V is the mass of the vector boson, is

$$i\mathcal{M}_{\varphi\varphi \rightarrow V\bar{V}} = (1)(-i\kappa v_0)(1)\frac{i}{q^2 - m_h^2 + im_h\Gamma_h}\varepsilon_\mu^*(p_V)\left(i\frac{2m_V g^{\mu\nu}}{v_0}\right)\varepsilon_\nu^*(p_{\bar{V}}). \quad (6.12)$$

The CM cross-section is then

$$\sigma_{\varphi\varphi \rightarrow V\bar{V}} = \frac{\delta_V}{16\pi s} \frac{\sqrt{1 - 4m_V^2/s}}{\sqrt{1 - 4m_\varphi^2/s}} \sum_{\text{polarization}} |\mathcal{M}_{\varphi\varphi \rightarrow V\bar{V}}|^2, \quad (6.13)$$

where δ_V (which equals 1 for the W boson and 1/2 for the Z boson) is a symmetry factor. Evaluating the sum over polarizations,

$$\begin{aligned} \sum_{\text{polarization}} |\mathcal{M}_{\varphi\varphi \rightarrow V\bar{V}}|^2 &= \frac{4\kappa^2 m_V^4}{(s - m_h^2)^2 + m_h^2 \Gamma_h^2} g^{\mu\nu} g^{\rho\sigma} \sum_{r,s} \varepsilon_\mu^{*r}(p_V) \varepsilon_\rho^r(p_V) \varepsilon_\nu^{*s}(p_{\bar{V}}) \varepsilon_\sigma^s(p_{\bar{V}}) \\ &= \frac{4\kappa^2 m_V^4}{(s - m_h^2)^2 + m_h^2 \Gamma_h^2} \left(\delta_\nu^\nu - \frac{p_V^2}{m_V^2} - \frac{p_{\bar{V}}^2}{m_V^2} + \frac{(p_V p_{\bar{V}})^2}{m_V^4} \right) \\ &= \frac{4\kappa^2 m_V^4}{(s - m_h^2)^2 + m_h^2 \Gamma_h^2} \left(2 + \frac{(s - 2m_V^2)^2}{4m_V^4} \right). \end{aligned} \quad (6.14)$$

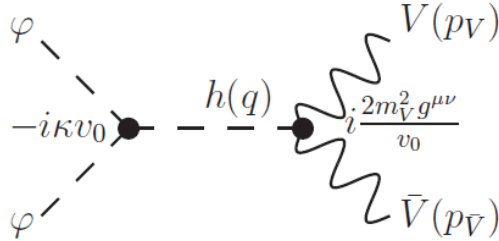


Figure 6.2: Dark Matter to Standard Model Vector Bosons, $\varphi\varphi \rightarrow V\bar{V}$

The cross-section is then

$$\sigma_{\varphi\varphi\rightarrow V\bar{V}} = \frac{\delta_V \kappa^2 m_V^4}{4\pi s} \frac{\sqrt{1 - 4m_V^2/s} (2 + (s - 2m_V^2)^2/4m_V^4)}{\sqrt{1 - 4m_\varphi^2/s} (s - m_h^2)^2 + m_h^2 \Gamma_h^2}. \quad (6.15)$$

Expanding the cross-section multiplied by v in powers of v we have

$$\sigma_{\varphi\varphi\rightarrow V\bar{V}} v = \sigma_{\varphi\varphi\rightarrow V\bar{V}}^{(0)} + \sigma_{\varphi\varphi\rightarrow V\bar{V}}^{(2)} v^2 + \mathcal{O}(v^4), \quad (6.16)$$

where

$$\sigma_{\varphi\varphi\rightarrow V\bar{V}}^{(0)} \equiv \frac{\delta_V \kappa^2}{32\pi m_\varphi^2} \frac{(1 - 4r_V^2)^{1/2} (1 - 2r_V^2 + 8r_V^4)}{(1 - r_h^2)^2 + r_\Gamma^2} \quad (6.17)$$

and

$$\sigma_{\varphi\varphi\rightarrow V\bar{V}}^{(2)} \equiv \frac{\delta_V \kappa^2 (1 - 4r_V^2)^{-1/2}}{64\pi m_\varphi^2 ((1 - r_h^2)^2 + r_\Gamma^2)^2} \left(-1 + 8r_V^2 - 26r_V^4 + 56r_V^6 + \dots \right. \\ \left. r_h^2 (1 - 10r_V^2 + 36r_V^4 - 80r_V^6) + 2r_V^2 (1 - 5r_V^2 + 12r_V^4) (r_h^4 + r_\Gamma^2) \right) \quad (6.18)$$

Dark Matter to Higgs Bosons, $\varphi\varphi \rightarrow hh$

Finally, the amplitude for the diagram in Figure 6.3 is

$$i\mathcal{M}_{\varphi\varphi\rightarrow hh} = (1)(1)(-i\kappa)(1)(1). \quad (6.19)$$

The above feynman diagram is the leading order DM annihilation process to two Higgs bosons. The s -channel diagram with a Higgs mediator and the t - and u -channel diagrams with a DM mediator being exchanged are sub-dominant to the four-vertex diagram.

Thus, the s -channel amplitude is

$$i\mathcal{M}_{\varphi\varphi\rightarrow hh}^{s\text{-channel}} = (1)(-i\kappa v_0)(1) \frac{i}{s - m_h^2 + im_h \Gamma_h} (1) \left(-i \frac{3m_h^2}{v_0} \right) (1), \quad (6.20)$$

which is considerable only near resonance. But at threshold, $v = 0$, and resonance (i.e. $2m_\varphi = m_h$) is kinematically forbidden since an on-shell Higgs boson cannot transmute to two Higgs bosons. Moreover, the t -channel amplitude (the u -channel is the same with the substitution $t \leftrightarrow u$) is

$$i\mathcal{M}_{\varphi\varphi\rightarrow hh}^{t\text{-channel}} = (1)(-i\kappa v_0)(1)\frac{i}{t - m_\varphi^2}(1)(-i\kappa v_0)(1), \quad (6.21)$$

where t (and u) is the Mandelstam variable, at threshold, $t = u = m_h^2 - m_\varphi^2$. The t/u -channels are only considerable when $m_h \approx \sqrt{2}m_\varphi$, which is kinematically forbidden.

The CM cross-section is then

$$\sigma_{\varphi\varphi\rightarrow hh} = \frac{1}{16\pi s} \frac{\sqrt{1 - 4m_h^2/s}}{\sqrt{1 - 4m_\varphi^2/s}} |\mathcal{M}_{\varphi\varphi\rightarrow hh}|^2 = \frac{\kappa^2}{16\pi s} \frac{\sqrt{1 - 4m_h^2/s}}{\sqrt{1 - 4m_\varphi^2/s}} \quad (6.22)$$

Expanding this cross-section multiplied by v in powers of v gives

$$\sigma_{\varphi\varphi\rightarrow hh}v = \sigma_{\varphi\varphi\rightarrow hh}^{(0)} + \sigma_{\varphi\varphi\rightarrow hh}^{(2)}v^2 + \mathcal{O}(v^4), \quad (6.23)$$

where

$$\sigma_{\varphi\varphi\rightarrow hh}^{(0)} \equiv \frac{\kappa^2}{64\pi m_\varphi^2} (1 - 4r_h^2)^{1/2} \quad (6.24)$$

and

$$\sigma_{\varphi\varphi\rightarrow hh}^{(2)} \equiv \frac{\kappa^2}{256\pi m_\varphi^2} \frac{(-1 + 6r_h^2)}{(1 - 4r_h^2)^{1/2}} \quad (6.25)$$

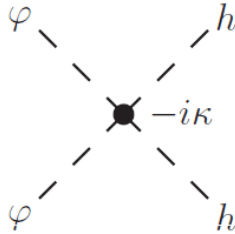


Figure 6.3: Dark Matter to Higgs Bosons, $\varphi\varphi \rightarrow hh$

6.2 Relic Density for the Scalar Higgs Portal

Now that we have derived analytic expressions for the leading contributions to the annihilation cross section we look to calculate the relic density of dark matter after freeze-out. As previously, to calculate the relic density we undertake a Boltzmann analysis as outlined in Section 3.3. Whereas previously we used simple parameterizations of the cross section, in working with a specific model there are a number of technicalities that one must take care of.

The Boltzmann equation is typically written in terms of the thermally-averaged cross-section $\langle\sigma_A v\rangle$ which is a product of the annihilation cross section and relative dark matter velocity averaged over the equilibrium distribution functions. More specifically, this quantity is defined as [62]

$$\langle\sigma_A v\rangle = \frac{1}{8m_\phi^4 T K_2^2(x)} \int_{4m_\phi^2}^{\infty} \sigma_A(s - 4m_\phi^2) \sqrt{s} K_1(\sqrt{s}/T) ds, \quad (6.26)$$

where we take σ_A to be

$$\sigma_A = \sum_{\text{SM particles}} \sigma_{\phi\phi\rightarrow ii}, \quad (6.27)$$

where the sum runs over the index ii of pairs of each type of Standard Model quark and lepton, the W and Z vector bosons and the Higgs boson. The mean speed of a particle at freeze-out ($x_F \sim 20$) is of order a third the speed of light, thus collecting terms up to order v^2 in the expansion of the annihilation cross-section provides a good approximation. Thermally averaging term-by-term gives [62]

$$\langle\sigma_A v\rangle = \langle\sigma_A^{(0)} + \sigma_A^{(2)} v^2 + \mathcal{O}(v^4)\rangle = \sigma_A^{(0)} + (3/2)\sigma_A^{(2)} x^{-1} + \mathcal{O}(x^{-2}), \quad (6.28)$$

where for ($j = 0, 2$),

$$\sigma_A^{(j)} \equiv \sum_{\text{SM particles}} \sigma_{\phi\phi\rightarrow ii}^{(j)}, \quad (6.29)$$

Applying this to the partial cross sections derived in the previous section, we plot in Figure 6.5 the total φ annihilation cross-section to Standard Model states via the Higgs portal (in units of the standard DM thermal cross-section: $\langle\sigma v\rangle_0 = 3(10)^{-26}\text{cm}^3/\text{s}$) for a fixed value $\kappa = 0.5$ of the mixed quartic. Additionally, in Figure 6.4 we show the fraction of the total annihilation cross-section at freeze-out going to various Standard Model particles for a fixed value $\kappa = 0.1$ of the mixed quartic $|H|^2|\varphi|^2$. In both cases we fix $\Gamma_h^{\text{SM}} = 13$ MeV which is consistent with current measurements [30]. Note that our independent analytic derivations of the Higgs partial annihilation rates, and the results presented in Figures 6.5 and 6.4 are in good agreement with related studies of the Higgs portal in the literature e.g. [63–66].

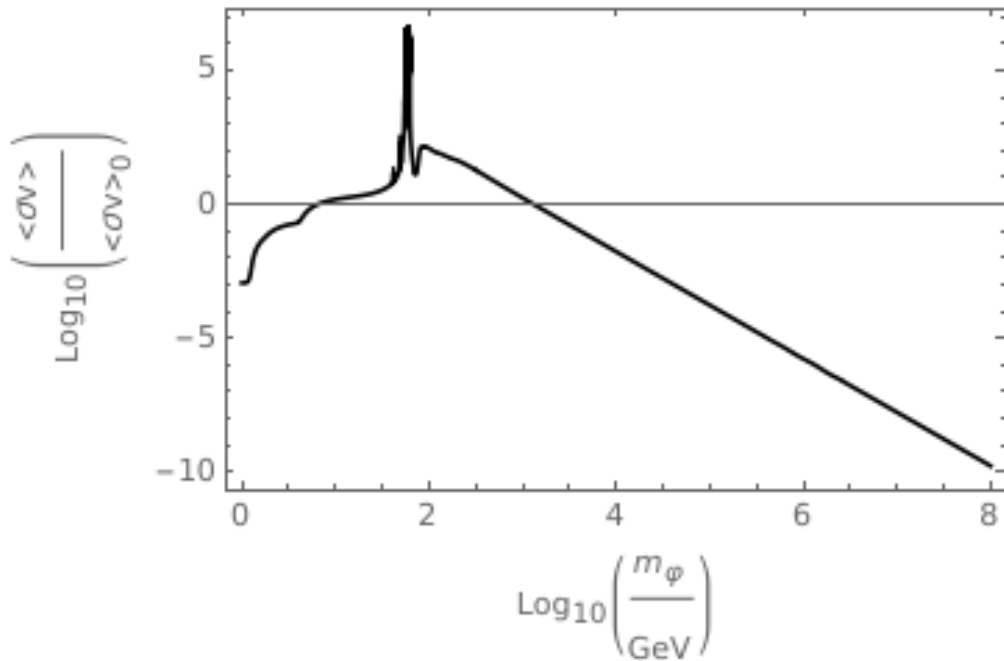


Figure 6.4: The total Higgs Portal annihilation cross-section in units of the standard DM relic density cross-section, $\langle\sigma v\rangle_0 = 3(10)^{-26}\text{cm}^3/\text{s}$, for a fixed value $\kappa = 0.5$ of the mixed quartic $|H|^2|\varphi|^2$, taking the Standard Model Higgs boson decay width to be $\Gamma_h^{\text{SM}} = 13$ MeV.

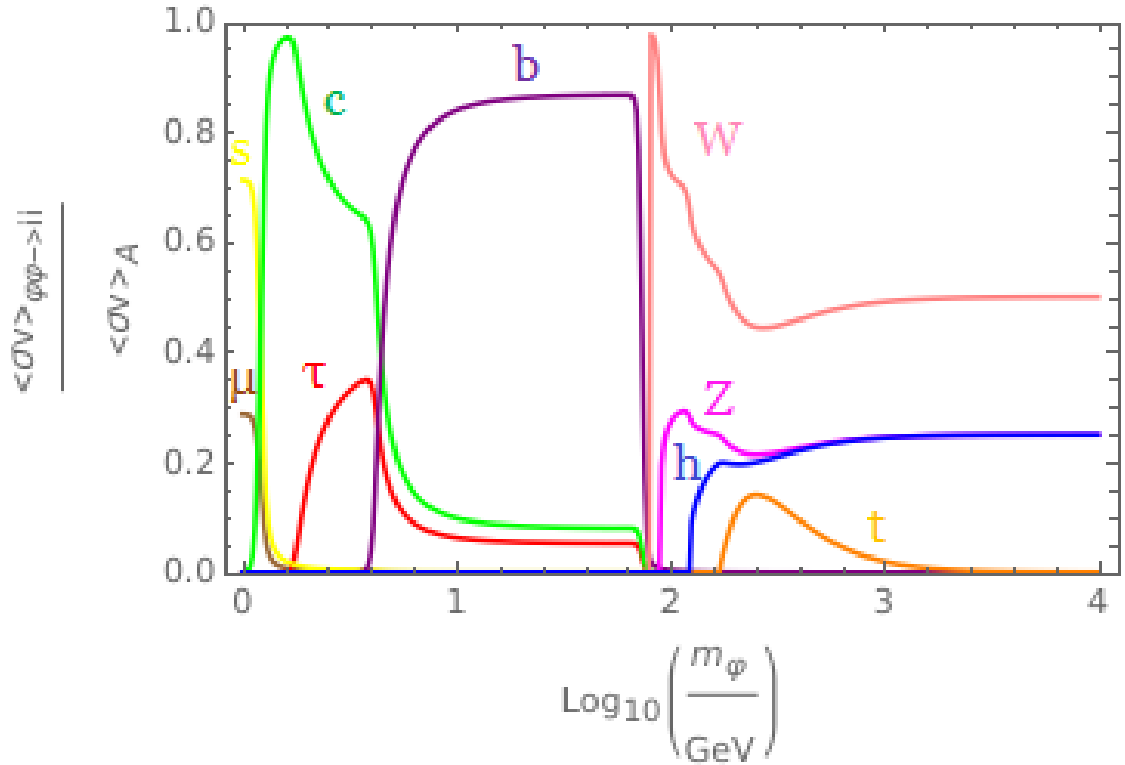


Figure 6.5: The fraction of the total annihilation cross-section at freeze-out going to various Standard Model particles for a fixed value $\kappa = 0.1$ of the mixed quartic $|H|^2|\varphi|^2$ and taking $\Gamma_h^{\text{SM}} = 13$ MeV. The curves indicate different Standard Model final state pairs: muons (brown), strange quarks (yellow), charm quarks (green), taus (red), bottom quarks (purple), W bosons (pink), Z bosons (magenta), Higgs Bosons (blue), and top quarks (orange).

With the appropriate thermally averaged cross section for the Higgs portal we can proceed to calculate the freeze-out temperature and subsequently the freeze-out abundance of dark matter. Using the freeze-out condition (3.2) with the cross-section (6.28), we have that freeze-out for the Higgs Portal, x_{F}^{HP} , occurs for

$$x_{\text{F}}^{\text{HP}} = \ln \left[\frac{gm_{\varphi}^3 \left(\sigma_{\text{A}}^{(0)} + (3/2)\sigma_{\text{A}}^{(2)} (x_{\text{F}}^{\text{HP}})^{-1} \right)}{(2\pi)^{3/2} H_{\star} x_{\star}^{3/2}} \left((1-r) + \frac{rx_{\star}}{(x_{\text{F}}^{\text{HP}})} \right)^{-1/2} \right]. \quad (6.30)$$

Taking an initial guess of $(x_{\text{F}}^{\text{HP}})^{(0)} = 1$, x_{F}^{HP} may be approximated as

$$(x_{\text{F}}^{\text{HP}})^{(1)} \equiv \ln \left[\frac{gm_{\varphi}^3 \left(\sigma_{\text{A}}^{(0)} + (3/2)\sigma_{\text{A}}^{(2)} \right)}{(2\pi)^{3/2} H_{\star} x_{\star}^{3/2}} ((1-r) + rx_{\star})^{-1/2} \right]. \quad (6.31)$$

Notice that κ^2 may be factored out of the cross-section in (6.31) giving

$$(x_{\text{F}}^{\text{HP}})^{(1)} = \ln \kappa^2 + (x_{\text{F}}^{\text{HP}})^{(1)} \Big|_{\kappa=1}, \quad (6.32)$$

which provides a compact expression for deriving constraints on κ and illustrates the freeze-out temperature is only logarithmically sensitive to changes in κ .

The only other relation that needs modification for the Higgs Portal is the abundance. Starting from eq. (3.24) and inserting the first two terms of (6.28), then following the line of argument used to derive (3.30), the freeze-out abundance for the Higgs Portal is

$$Y_{\infty}^{\text{HP}} \approx \left[\tilde{\lambda} (1-r)^{-1/2} \left(\sigma_{\text{A}}^{(0)} \int_{x_{\text{F}}}^{\infty} dx \left(1 + \frac{r}{(1-r)} \frac{x_{\star}}{x} \right)^{-1/2} x^{-5/2} + \dots \right. \right. \\ \left. \left. (3/2)\sigma_{\text{A}}^{(2)} \int_{x_{\text{F}}}^{\infty} dx \left(1 + \frac{r}{(1-r)} \frac{x_{\star}}{x} \right)^{-1/2} x^{-7/2} \right) \right]^{-1} \quad (6.33)$$

where,

$$\tilde{\lambda} \equiv \frac{2\pi^2 g_{\star} s m_{\varphi}^3}{45 H_{\star} x_{\star}^{3/2}}. \quad (6.34)$$

The analytic form for Y_∞^{HP} is unwieldy, however it is interesting to note that by writing $\tilde{a} \equiv rx_\star/(1-r)x_{\text{F}}$, the integrals in (6.33) can be evaluated analytically,

$$\int_{x_{\text{F}}}^{\infty} dx \left(1 + \frac{r}{(1-r)} \frac{x_\star}{x}\right)^{-1/2} x^{-5/2} = \left(\frac{1-r}{rx_\star}\right)^{3/2} \left(\sqrt{\tilde{a}(1+\tilde{a})} - \text{arcsinh} \sqrt{\tilde{a}}\right) \quad (6.35)$$

and

$$\begin{aligned} \int_{x_{\text{F}}}^{\infty} dx \left(1 + \frac{r}{(1-r)} \frac{x_\star}{x}\right)^{-1/2} x^{-7/2} \\ = \left(\frac{3}{4}\right) \left(\frac{1-r}{rx_\star}\right)^{5/2} \left(\sqrt{\tilde{a}(1+\tilde{a})}((2/3)\tilde{a} - 1) + \text{arcsinh} \sqrt{\tilde{a}}\right). \end{aligned} \quad (6.36)$$

Similar to the model independent analysis (cf. eq. (3.38)) the freeze-out abundance is diluted as $\Omega_{\text{DM}}^{\text{relic}} h^2 = \zeta \Omega_{\text{DM}}^{\text{F}} h^2$. Conversely the to match the observed relic density one requires

$$\zeta = \frac{\Omega_\varphi^{\text{relic}} h^2}{\Omega_\varphi^{\text{HP}} h^2} = \frac{\rho_{\text{critical}} \Omega_\varphi^{\text{relic}} h^2}{s_0 m_\varphi Y_\infty^{\text{HP}}} \quad (6.37)$$

Note that ζ is related to T_{RH} via eq. (3.55). In Figure 6.6 we display contours of the T_{RH} which give the correct relic density for scalar dark matter freezing out via the Higgs portal. This plot is overlaid with theoretical constraints, similar to those explored in Chapter 4, which we discuss in the next section.

6.3 Theoretical Constraints

In Chapter 4 we studied the theoretical constraints on the matter dominated freeze-out scenario in a model independent manner, here we re-examine these requirements in the specific context of the scalar Higgs Portal. In the plots which appear at the end of this section we will use the full expression for Y_∞^{HP} , however to gain some intuition it will be insightful to make a minor approximation and derive some bounds on the various parameters analytically.

Specifically, we consider a quantity \hat{Y} in which we factor out the explicit κ dependence from Y_∞^{HP} as follows

$$\hat{Y} = \frac{Y_\infty^{\text{HP}}}{\kappa^2} \propto x_F^{\text{HP}}. \quad (6.38)$$

As noted in eq. (6.32) the freeze-out (inverse) temperature x_F^{HP} is only logarithmically sensitive to κ , thus the principal κ dependence in Y_∞^{HP} is due to the explicit factor. For the purpose of arriving at reasonable analytic bounds on this scenario we will treat \hat{Y} as independent of κ , and neglect the logarithmic dependence due to x_F^{HP} , which we fix at the characteristic value $\hat{x}_F \approx 20$. The dependence of x_F^{HP} will be restored when we re-examine these constraints in Figure 6.6.

Emulating the study in Chapter 4, below we look at the leading theoretical constraints on this scenario,

- Freeze-out of dark matter before decay of Φ matter.
- Freeze-out of dark matter during matter domination.
- Sufficiently high reheat temperature from Φ Decays.

In this case, however, we use these constraints to derive bounds on the portal coupling κ which dresses the mixed quartic coupling $\frac{1}{2}\kappa\varphi^2 H^\dagger H$. We also check the constraints coming from unitarity and perturbativity here.

In Chapter 4 we derived that the theoretical requirement that dark matter freeze-out occurs before the decay of Φ can be expressed as a bound on T_\star as follows $T_\star \gtrsim \frac{x_F^3}{(1-r)\hat{\gamma}} \frac{T_{\text{RH}}^4}{m_\varphi^3}$, see eq. (4.9) and recall here $\hat{\gamma}$ is defined in eq. (3.51). In the context of the Higgs portal this constraint can be written as a constraint on the coupling

$$\kappa \lesssim \left[\frac{r^{4/3}\hat{\gamma}^{1/3}m_\varphi}{(1-r)\hat{x}_F T_\star} \right]^{3/8} \left(\frac{s_0 m_\varphi \hat{Y}}{\rho_{\text{critical}} \Omega_\varphi^{\text{relic}} h^2} \right)^{1/2} \quad (6.39)$$

This constraint is shown in Figure 6.6 (with the full κ dependence) as the purple curve.

Moreover, recall from Chapter 5 that if freeze-out occurs near $H \sim \Gamma_\Phi$ then there is loss of entropy conservation in the bath which significantly alters the physics. Thus

to remain in the matter dominated freeze-out regime we require that $T_F \gtrsim T_{EV}$, where eq. (5.23) gives the temperature of entropy violation T_{EV} . Note that if this is satisfied then the instantaneous decay approximation for Φ decays is a good approximation.

The constraint $T_F \gtrsim T_{EV}$ can be expressed in terms of κ as follows

$$\kappa^{8/5} \lesssim \left(\frac{5}{3\hat{\gamma}^{1/2}} \right)^{2/5} \left(\frac{r}{1-r} \right)^{6/5} \left(\frac{s_0 m_\varphi \hat{Y}}{\rho_{\text{critical}} \Omega_\varphi^{\text{relic}} h^2} \right)^{4/5} \frac{m_\varphi}{T_\star \hat{x}_F} \quad (6.40)$$

This is shown in Figure 6.6 as the yellow curve (including the full κ dependence).

Next we constrain the parameter space to those parts in which dark matter freeze-out occurs during matter domination, comparing with eq. (4.7) in Chapter 4 this can be expressed as $T_\star \gtrsim \frac{r}{(1-r)} \frac{m_\varphi}{3\beta x_F}$ and in terms of κ implies

$$\kappa^2 \gtrsim \exp \left[\frac{r}{(1-r)} \frac{m_\varphi}{3\beta T_\star} - \hat{x}_F \right] \quad (6.41)$$

This is shown in Figure 6.6 as the red curve (including the full κ dependence).

Furthermore, there is the requirement that to reproduce the successes of early universe cosmology, the temperature after Φ decays is above the temperature of BBN $T_{\text{BBN}} \sim 10$ MeV. Using (6.37) and eq. (3.55), the constraint $T_{\text{RH}} \gtrsim T_{\text{BBN}}$ implies

$$\kappa^2 \gtrsim \frac{r}{1-r} \left(\frac{s_0 m_\varphi \hat{Y}}{\rho_{\text{critical}} \Omega_\varphi^{\text{relic}} h^2} \right) \frac{T_{\text{BBN}}}{T_\star} \quad (6.42)$$

This is shown in Figure 6.6 as the blue curve (including the full κ dependence).

In addition to the reheat temperature being above T_{BBN} we also require that $T_{\text{RH}} \lesssim T_F$, to ensuring that the dark matter is not re-populated by the thermal bath as the expansion rate changes, as discussed in Section 4.3. Specifically, the requirement that $T_{\text{RH}} \lesssim T_F$ may be expressed as follows

$$\kappa^2 \lesssim \frac{r}{1-r} \left(\frac{s_0 m_\varphi \hat{Y}}{\rho_{\text{critical}} \Omega_\varphi^{\text{relic}} h^2} \right) \frac{m_\varphi}{T_\star \hat{x}_F} \quad (6.43)$$

This is shown in Figure 6.6 as the green curve (including the full κ dependence).

It is also worth highlighting that the dark matter unitarity constraint, due to Griest and Kamionkowski [67], is greatly relaxed in this scenario. Although the limit on plane wave unitarity persists, namely that the maximum cross-section derived from unitarity consideration is $\langle\sigma v\rangle_{\max} = 4\pi\sqrt{x_F}/\sqrt{6}m_\varphi^2$ [67], since $\Omega_\varphi^{\text{relic}}h^2 \ll \Omega_\varphi^{\text{F}}h^2$ due to the entropy injection, the freeze-out abundance can be much larger than the standard freeze-out abundance without overclosing the universe. While a dark matter unitarity constraint still exists it does not effectively constrain either plot of Figure 6.6. Additionally, since we have treated this model perturbatively, there is a requirement of perturbative couplings, thus we require that $\kappa \lesssim \sqrt{4\pi}$, and to illustrate this constraint in Figure 6.6 we cut the κ axis at $\kappa = \sqrt{4\pi}$.

We collect these constraints in Figure 6.6 for two values of the critical temperature T_\star at which Φ becomes matter like, and where we fix $r = 0.99$. Observe that the theoretical requirements effectively constrain the parameter space, but leave a modest range of parameters in which matter dominated dark matter freeze-out via the scalar Higgs portal can be successfully realized.

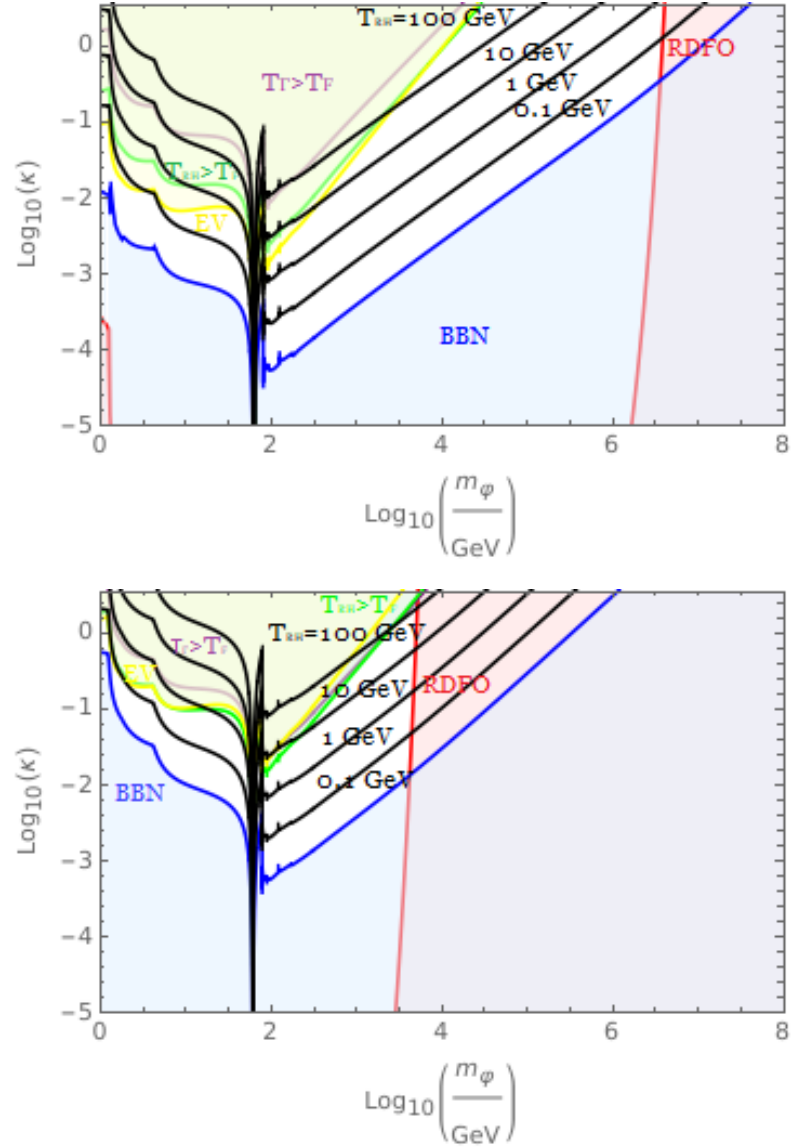


Figure 6.6: Dominant constraints and relic density contours for $r = 0.99$, $T_\star = 10^7 \text{ GeV}$ (upper) and $T_\star = 10^4$ (lower). Shaded regions excluded due to BBN constraint (blue), MD FO (red), decay before FO (purple), non-adiabaticity (yellow), and no re-population (green). From bottom to top of graph, the black contours give the correct relic density for $T_{RH} = 0.1 \text{ GeV}$, 1 GeV , 10 GeV , and 100 GeV .

6.4 Experimental Constraints

In the previous section we argued that matter dominated freeze-out via the Higgs portal is theoretically viable in modest parameter regions, and we now turn to the experimental limits. First we consider direct detection experiments which rely on DM particles interacting with various nuclei [30]. These experiments look for signals from the recoil that a nuclei would undergo in the event that it interacted with DM, thus providing considerable constraints on DM parameters [63]. The DM parameters that these experiments exclude for the Higgs model we study may be seen above the dashed magenta (XENON1T [68]) and blue (LUX [69] and PandaX [70]) lines in Figure 6.8. To translate the cross-section bounds of these experiments into Higgs Portal terms, we used the common parameterization for spin-independent DM-nucleon scattering [71, 72],

$$\sigma_{\varphi-N}^{\text{SI}} \simeq \frac{\kappa^2}{4\pi m_h^4} \frac{m_N^4 f_N^2}{(m_\varphi + m_N)^2} \quad (6.44)$$

where the nucleon mass is $m_N \approx 1$ GeV, and the hadronic matrix element parameter $f_N = 0.326$ [71, 73]. Note that future experiments with improved sensitivity will need to confront the difficult task of distinguishing neutrino signals from DM signals in the region termed the “neutrino floor,” indicated as the green dashed line in Figure 6.8.

Indirect detection of DM experiments rely on detecting the products of DM annihilations that may occur, for instance, in the Milky Way galaxy center or near the Sun where DM concentrations are expected to be higher than average [30]. For example, the Fermi-LAT collaboration’s [74] data from observing DM annihilations into the $b\bar{b}$ channel moderately constrains the allowable parameter space for the Higgs portal [63]. In our model, the excluded parameters from this indirect experimental data is seen in Figure 6.8 as the orange shaded region above the dashed orange line. Figure 6.8 also shows that indirect experiments are currently less constraining than other experimental methods.

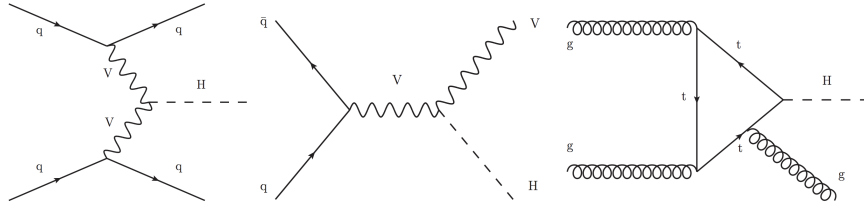


Figure 6.7: Figure from V. Khachatryan *et al.* [37]. The Figure illustrates the three production processes targeted in the CMS search for invisible Higgs boson decays.

Another experimental method for probing DM is through collider searches e.g. [32–35]. If DM interacts with the SM, one would expect that a fraction of the high energy particle collisions would produce DM. By measuring the energy of the products of particle collisions, it may be inferred if there are invisible states which carry away energy undetected through the experimental triggers. For the Higgs Portal, the Higgs width is the relevant parameter to probe. Specifically, emulating [63], we compare with the CMS search for invisible decays of the Higgs boson in pp collisions at $\sqrt{s} = 7, 8,$ and 13 TeV [37], the processes targeted in this search are shown in Figure 6.7. The current branching fraction of the Higgs width that may go to an invisible state is constrained by the Large Hadron Collider (LHC) searches as, $\mathcal{B}(h \rightarrow \text{inv}) \equiv \Gamma_{\text{inv}}/(\Gamma_{\text{inv}} + \Gamma_{\text{SM}}) < 0.2$ with 90% confidence level [37]. Assuming that the invisible decays are due to DM and using eq. (6.4), this gives a constraint on Higgs portal DM as illustrated by region above the red dashed line in Figure 6.8.

In Figure 6.8 we collect both the experimental and theoretical limits together; while this scenario is quite constrained in the low-mass/high-coupling regime shown in the figure, viable parameter space remains. Notably, radiation dominated freeze-out via the Higgs portal (without an entropy injection) is largely excluded apart from around the region of resonant annihilation as indicated by the black dashed line in Figure 6.8 (also see e.g. [63]). Thus it is interesting to observe that the classic Higgs portals returns as a possibility for providing the correct dark matter abundance, while avoiding constraints for models with an entropy injection such as matter dominated dark matter freeze-out.

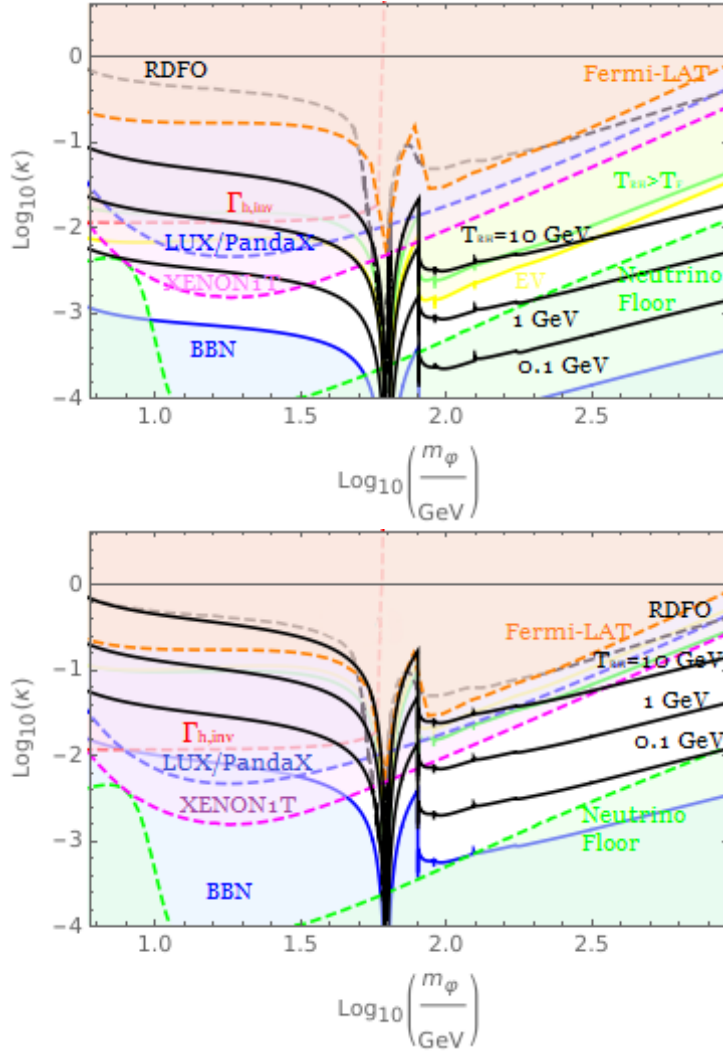


Figure 6.8: Experimental (dashed lines) and theoretical (solid lines) bounds for $r = 0.99$, $T_* = 10^7$ GeV (upper) and $T_* = 10^4$ GeV (lower). For experimental constraints, shaded regions excluded from XENON1T [68] (above dashed magenta line), LUX [69] and PandaX [70] (above dashed blue line), and Fermi-LAT [74] indirect detection experiment (above dashed orange line). The black dashed line is the standard RD FO scenario contour for matching the observed DM relic density [63]. For theoretical constraints, shaded regions excluded due to BBN constraint (above solid blue line), non-adiabaticity (above solid yellow line), and no re-population (above solid green line). Green dashed line indicates the “neutrino floor”. From bottom to top the black contours give the correct relic density for $T_{RH} = 0.1$ GeV, 1 GeV, and 10 GeV.

Chapter 7

Conclusion

This chapter presents a summary and discussion of the results of this thesis.

Dark matter poses one of the greatest and most exciting challenges for science today. Since the 1930s we have known that something was amiss with our description of the universe. As more data and theoretical work has accumulated, the Λ CDM model, of which dark matter is a critical component, has provided compelling explanations for the disparate phenomenon we observe in our universe. In this thesis we made the case for dark matter in Chapter 1, and described the empirical searches for particle dark matter, which laid the ground for the validity of our investigation. Indeed it was shown how Λ CDM explains the galactic rotation curves, the baryon budget, the CMB power spectrum, large scale structure formation, and the Bullet Cluster in a coherent manner. With such powerful explanatory power, vigorous empirical effort has been made including efforts at direct detection, indirect detection, and collider searches.

It is vital that our empirical efforts are guided with the light of rigorous theoretical work. In Chapter 2 we laid out the plausible scenario that dark matter may have undergone freeze-out during an era of the universe in which matter was dominant. There we discussed the possibility that $T_{\text{MD}} \gg T_F \gg T_\Gamma$ and $H \propto T^{3/2}$ during freeze-out, as well as how the different dynamics and constituency of the universe may impact dark matter. The following two chapters were devoted to exploring this scenario rigorously and

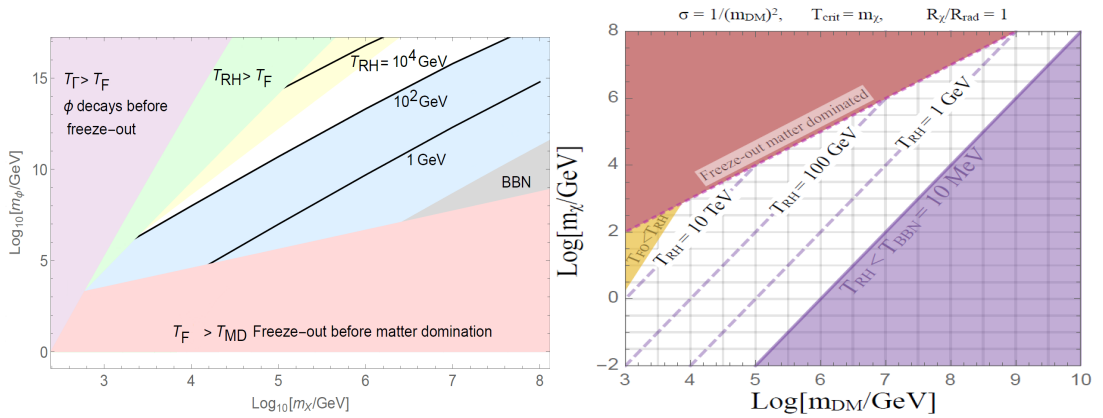


Figure 7.1: Left panel is Figure 4.1 of this thesis. Right panel is figure from J. Bramante and J. Unwin JHEP 1702 (2017) 119 [39].

investigating its prominent constraints. In Chapter 5 we demonstrated that the instantaneous decay approximation we used for simplicity was well justified, and showed the regions of parameter space where it may break down. Finally in Chapter 6 the viability of a matter-dominated freeze-out scenario was well established with our presentation of how it re-opens wide the hitherto claimed, nearly “closed” Higgs Portal

This thesis initially grew out of considering what may lie in the red region of the right panel of Figure 7.1 from J. Bramante and J. Unwin’s work [39] in which traditional freeze-out calculations broke-down. This thesis shows it is both a viable and rich region of parameter space, as it is elucidated in the left panel of Figure 7.1, which is even capable of reviving hitherto excluded models of dark matter, such as the Higgs Portal. Future work will further investigate the rich possibilities that matter-dominated freeze-out creates, and studying this scenario is an essential step forward in our understanding of the range of possibilities for consistent and compelling models of dark matter.

Bibliography

- [1] S. Hamdan and J. Unwin, *Dark Matter Freeze-out During Matter Domination*, arXiv:1710.03758 [hep-ph].
- [2] C. L. Bennett *et al.* [WMAP Collaboration], *Nine-Year Wilkinson Microwave Anisotropy Probe (WMAP) Observations: Final Maps and Results*, *Astrophys. J. Suppl.* **208** (2013) 20 [1212.5225].
- [3] G. Bertone, D. Hooper and J. Silk, *Particle dark matter: Evidence, candidates and constraints*, *Phys. Rept.* **405** (2005) 279 [hep-ph/0404175].
- [4] B. W. Lee and S. Weinberg, *Cosmological Lower Bound on Heavy Neutrino Masses*, *Phys. Rev. Lett.* **39** (1977) 165.
- [5] E. W. Kolb and M. S. Turner, *The Early Universe*, *Front. Phys.* **69** (1990) 1.
- [6] G. F. Giudice, E. W. Kolb and A. Riotto, *Largest temperature of the radiation era and its cosmological implications*, *Phys. Rev. D* **64** (2001) 023508 [hep-ph/0005123].
- [7] J. McDonald, *WIMP Densities in Decaying Particle Dominated Cosmology*, *Phys. Rev. D* **43** (1991) 1063.
- [8] G. Bertone and D. Hooper, *A History of Dark Matter*, [1605.04909].
- [9] F. Zwicky, *Die Rotverschiebung von extragalaktischen Nebeln*, *Helv. Phys. Acta* **6**, 110 (1933) [*Gen. Rel. Grav.* **41**, 207 (2009)].
- [10] V. C. Rubin, N. Thonnard and W. K. Ford, Jr., *Rotational properties of 21 SC galaxies with a large range of luminosities and radii, from NGC 4605 / $R = 4\text{kpc}$ / to UGC 2885 / $R = 122\text{kpc}$ /*, *Astrophys. J.* **238**, 471 (1980).
- [11] K. G. Begeman, A. H. Broeils and R. H. Sanders, *Extended rotation curves of spiral galaxies: Dark haloes and modified dynamics*, *Mon. Not. Roy. Astron. Soc.* **249**, 523 (1991).
- [12] M. Lisanti, *Lectures on Dark Matter Physics*, [1603.03797].
- [13] T. S. van Albada, J. N. Bahcall, K. Begeman and R. Sancisi, *The Distribution of Dark Matter in the Spiral Galaxy NGC-3198*, *Astrophys. J.* **295** (1985) 305.

- [14] D. J. Hegyi and K. A. Olive, *Can Galactic Halos Be Made of Baryons?*, Phys. Lett. B **126**, 28 (1983) [Phys. Lett. **126B**, 28 (1983)].
- [15] P. Tisserand *et al.* [EROS-2 Collaboration], *Limits on the Macho Content of the Galactic Halo from the EROS-2 Survey of the Magellanic Clouds*, Astron. Astrophys. **469**, 387 (2007) [astro-ph/0607207].
- [16] G. Bertone *et al.*, *Particle Dark Matter: Observations, Models and Searches*.
- [17] P. A. R. Ade *et al.* [Planck Collaboration], *Planck 2015 results. XIII. Cosmological parameters*, Astron. Astrophys. **594**, A13 (2016) [1502.01589].
- [18] W. Hu and S. Dodelson, *Cosmic microwave background anisotropies*, Ann. Rev. Astron. Astrophys. **40**, 171 (2002) [astro-ph/0110414].
- [19] P. J. E. Peebles, *Large scale background temperature and mass fluctuations due to scale invariant primeval perturbations*, Astrophys. J. **263**, L1 (1982).
- [20] M. Davis, G. Efstathiou, C. S. Frenk and S. D. M. White, *The Evolution of Large Scale Structure in a Universe Dominated by Cold Dark Matter*, Astrophys. J. **292**, 371 (1985).
- [21] M. Vogelsberger *et al.*, *Properties of galaxies reproduced by a hydrodynamic simulation*, Nature **509**, 177 (2014) [1405.1418].
- [22] J. Schaye *et al.*, *The EAGLE project: Simulating the evolution and assembly of galaxies and their environments*, Mon. Not. Roy. Astron. Soc. **446**, 521 (2015) [1407.7040].
- [23] J. F. Navarro, C. S. Frenk and S. D. M. White, *The Structure of cold dark matter halos*, Astrophys. J. **462**, 563 (1996) [astro-ph/9508025].
- [24] S. D. M. White, C. S. Frenk and M. Davis, *Clustering in a Neutrino Dominated Universe*, Astrophys. J. **274**, L1 (1983).
- [25] D. Clowe, M. Bradac, A. H. Gonzalez, M. Markevitch, S. W. Randall, C. Jones and D. Zaritsky, *A direct empirical proof of the existence of dark matter*, Astrophys. J. **648**, L109 (2006) [astro-ph/0608407].
- [26] S. Tremaine, *A Historical Perspective on Dark Matter*, Dark matter in the universe, Vol. 117, IAU Symposium (1987)
- [27] J. Einasto, *Dark matter*, Baltic Astron. **20**, 231 (2011) [1109.5580]
- [28] M. Milgrom, *A Modification of the Newtonian dynamics as a possible alternative to the hidden mass hypothesis*, Astrophys. J. **270**, 365 (1983).
- [29] G. Arcadi, M. Dutra, P. Ghosh, M. Lindner, Y. Mambrini, M. Pierre, S. Profumo and F. S. Queiroz, *The waning of the WIMP? A review of models, searches, and constraints*, Eur. Phys. J. C **78**, no. 3, 203 (2018) [1703.07364].

- [30] M. Tanabashi *et al.* [Particle Data Group], *Review of Particle Physics*, Phys. Rev. D **98**, 030001 (2018).
- [31] F. Kahlhoefer, *Review of LHC Dark Matter Searches*, Int. J. Mod. Phys. A **32**, no. 13, 1730006 (2017) [1702.02430].
- [32] P. J. Fox, R. Harnik, J. Kopp and Y. Tsai, *LEP Shines Light on Dark Matter*, Phys. Rev. D **84** (2011) 014028 [1103.0240].
- [33] A. Rajaraman, W. Shepherd, T. M. P. Tait and A. M. Wijangco, *LHC Bounds on Interactions of Dark Matter*, Phys. Rev. D **84** (2011) 095013 [1108.1196].
- [34] P. J. Fox, R. Harnik, J. Kopp and Y. Tsai, *Missing Energy Signatures of Dark Matter at the LHC*, Phys. Rev. D **85** (2012) 056011 [1109.4398].
- [35] U. Haisch, F. Kahlhoefer and J. Unwin, *The impact of heavy-quark loops on LHC dark matter searches*, JHEP **1307** (2013) 125 [1208.4605].
- [36] T. Plehn, *Yet Another Introduction to Dark Matter*, arXiv:1705.01987.
- [37] V. Khachatryan *et al.* [CMS Collaboration], *Searches for invisible decays of the Higgs boson in pp collisions at $\sqrt{s} = 7, 8, \text{ and } 13 \text{ TeV}$* , JHEP **1702**, 135 (2017) [1610.09218].
- [38] S. Weinberg, *Cosmology*, Oxford, UK: Oxford Univ. Pr. (2008) 593 p
- [39] J. Bramante and J. Unwin, *Superheavy Thermal Dark Matter and Primordial Asymmetries*, JHEP **1702** (2017) 119 [1701.05859].
- [40] R. J. Scherrer and M. S. Turner, *Decaying Particles Do Not Heat Up the Universe*, Phys. Rev. D **31** (1985) 681.
- [41] M. Kamionkowski and M. S. Turner, *Thermal Relics: Do We Know Their Abundances?*, Phys. Rev. D **42** (1990) 3310.
- [42] R. T. Co, F. D'Eramo, L. J. Hall and D. Pappadopulo, *Freeze-In Dark Matter with Displaced Signatures at Colliders*, JCAP **1512** (2015) no.12, 024 [1506.07532].
- [43] D. J. H. Chung, E. W. Kolb and A. Riotto, *Production of massive particles during reheating*, Phys. Rev. D **60** (1999) 063504 [hep-ph/9809453].
- [44] G. B. Gelmini and P. Gondolo, *Neutralino with the right cold dark matter abundance in (almost) any supersymmetric model*, Phys. Rev. D **74** (2006) 023510 [hep-ph/0602230].
- [45] L. Randall, J. Scholtz and J. Unwin, *Flooded Dark Matter and S Level Rise*, JHEP **1603** (2016) 011 [1509.08477].
- [46] A. Berlin, D. Hooper and G. Krnjaic, *PeV-Scale Dark Matter as a Thermal Relic of a Decoupled Sector*, Phys. Lett. B **760**, 106 (2016) [1602.08490].

- [47] A. Mitridate, M. Redi, J. Smirnov and A. Strumia, *Dark Matter as a weakly coupled Dark Baryon*, [1707.05380].
- [48] F. D’Eramo, N. Fernandez and S. Profumo, *When the Universe Expands Too Fast: Relentless Dark Matter*, JCAP **1705** (2017) no.05, 012 [1703.04793].
- [49] B. Spokoiny, *Deflationary universe scenario*, Phys. Lett. B **315** (1993) 40 [gr-qc/9306008].
- [50] K. Redmond and A. L. Erickcek, *New Constraints on Dark Matter Production during Kination*, Phys. Rev. D **96** (2017) no.4, 043511 [1704.01056].
- [51] J. Bernstein, L. S. Brown and G. Feinberg, *The Cosmological Heavy Neutrino Problem Revisited*, Phys. Rev. D **32**, 3261 (1985).
- [52] R. Scherrer and M. Turner, *On the Relic, Cosmic Abundance of Stable Weakly Interacting Massive Particles*, Phys. Rev. D **33** (1986) 1585. [Erratum: Phys. Rev. D **34**, 3263 (1986)].
- [53] M. Taoso, G. Bertone and A. Masiero, *Dark Matter Candidates: A Ten-Point Test*, JCAP **0803**, 022 (2008) [0711.4996].
- [54] D. E. Morrissey and M. J. Ramsey-Musolf, *Electroweak baryogenesis*, New J. Phys. **14** (2012) 125003 [1206.2942].
- [55] V. Silveira and A. Zee, *Scalar Phantoms*, Phys. Lett. **161B** (1985) 136.
- [56] J. McDonald, *Gauge singlet scalars as cold dark matter*, Phys. Rev. D **50** (1994) 3637 [hep-ph/0702143].
- [57] C. P. Burgess, M. Pospelov and T. ter Veldhuis, *The Minimal model of nonbaryonic dark matter: A Singlet scalar*, Nucl. Phys. B **619** (2001) 709 [hep-ph/0011335].
- [58] B. Patt and F. Wilczek, *Higgs-field portal into hidden sectors*, hep-ph/0605188.
- [59] S. L. Glashow, “Partial Symmetries of Weak Interactions,” Nucl. Phys. **22** (1961) 579.
- [60] S. Weinberg, “A Model of Leptons,” Phys. Rev. Lett. **19** (1967) 1264.
- [61] A. Salam, in: Elementary Particle Theory, ed. N. Svartholm, Almquist and Wiksell, (1968) 367.
- [62] P. Gondolo and G. Gelmini, *Cosmic abundances of stable particles: Improved analysis*, Nucl. Phys. B **360**, 145 (1991).
- [63] M. Escudero, A. Berlin, D. Hooper and M. X. Lin, *Toward (Finally!) Ruling Out Z and Higgs Mediated Dark Matter Models*, JCAP **1612**, 029 (2016) [1609.09079].

- [64] J. M. Cline and K. Kainulainen, *Electroweak baryogenesis and dark matter from a singlet Higgs*, JCAP **1301** (2013) 012 [1210.4196].
- [65] J. M. Cline, K. Kainulainen, P. Scott and C. Weniger, *Update on scalar singlet dark matter*, Phys. Rev. D **88** (2013) 055025 Erratum: [Phys. Rev. D **92** (2015) no.3, 039906] [1306.4710].
- [66] L. Feng, S. Profumo and L. Ubaldi, *Closing in on singlet scalar dark matter: LUX, invisible Higgs decays and gamma-ray lines*, JHEP **1503** (2015) 045 [1412.1105].
- [67] K. Griest and M. Kamionkowski, *Unitarity Limits on the Mass and Radius of Dark Matter Particles*, Phys. Rev. Lett. **64** (1990) 615.
- [68] E. Aprile *et al.* [XENON Collaboration], *Dark Matter Search Results from a One Tonne \times Year Exposure of XENON1T*, [1805.12562].
- [69] D. S. Akerib *et al.* [LUX Collaboration], *Results from a search for dark matter in the complete LUX exposure*, Phys. Rev. Lett. **118**, no. 2, 021303 (2017) [1608.07648].
- [70] A. Tan *et al.* [PandaX-II Collaboration], *Dark Matter Results from First 98.7 Days of Data from the PandaX-II Experiment*, Phys. Rev. Lett. **117**, no. 12, 121303 (2016) [1607.07400].
- [71] A. Djouadi, O. Lebedev, Y. Mambrini and J. Quevillon, *Implications of LHC searches for Higgs-portal dark matter*, Phys. Lett. B **709**, 65 (2012) [1112.3299].
- [72] S. Kanemura, S. Matsumoto, T. Nabeshima and N. Okada, *Can WIMP Dark Matter overcome the Nightmare Scenario?*, Phys. Rev. D **82**, 055026 (2010) [1005.5651].
- [73] R. D. Young and A. W. Thomas, *Octet baryon masses and sigma terms from an $SU(3)$ chiral extrapolation*, Phys. Rev. D **81**, 014503 (2010) [0901.3310].
- [74] M. Ackermann *et al.* [Fermi-LAT Collaboration], *Searching for Dark Matter Annihilation from Milky Way Dwarf Spheroidal Galaxies with Six Years of Fermi Large Area Telescope Data*, Phys. Rev. Lett. **115**, no. 23, 231301 (2015) [1503.02641].